Electronic Supplementary Information

Design of Ionic Liquid Crystals Enabled by [2]Rotaxane Structure Formation

Gosuke Washino[a], Takashi Kajitani[b], Suzushi Nishimura[c], and Atsushi Shishido*[a,d]

a. Laboratory for Chemistry and Life Science, Institute of Innovative Research, Tokyo Institute of Technology, 4259 Nagatsuta, Midori-ku, Yokohama 226-8501, Japan.
b. Open Facility Center, Tokyo Institute of Technology, 4259 Nagatsuta, Midori-ku, Yokohama 226-8501, Japan.
c. School of Materials and Chemical Technology, Tokyo Institute of Technology, 4259 Nagatsuta, Midori-ku, Yokohama 226-8501, Japan.
d. Research Center for Autonomous Systems Materialogy, Institute of Innovative Research, Tokyo Institute of Technology, 4259 Nagatsuta, Midori-ku, Yokohama 226-8501, Japan.

Email: ashishid@res.titech.ac.jp

1. General Information

All commercially available chemicals were purchased from Tokyo Chemical Industry (TCI) and FUJIFILM Wako Pure Chemical Corporation and used as received. Flash column chromatography was performed using an automated chromatography system employing Yamazen Corporation Isolera-4 or Isolera-1 automated chromatography system (Yamazen Corporation W-Prep 2XY) and Universal Column cartridges (40 μm silica). Nuclear magnetic resonance (NMR) experiments were recorded on Bruker AVANCE 400 MHz spectrometers; ^{1}H and ^{13}C NMR chemical shifts (δ) are given in parts per million (ppm) relative to tetramethylsilane as referenced with the residual solvent signal. J values are reported in Hz, and signal multiplicity is denoted as s (singlet), d (doublet), t (triplet), dd (doublet of doublet), quin (quintet) m (multiplet), and br (broad signal). UV-vis spectra were recorded on a JASCO V-670 spectrometer. The samples were prepared as film shapes obtained by sandwiching them between glass slides that had been ultrasonically cleaned in IPA and heated above their melting point. The measurements were performed through glass substrates. Electrospray ionization - high-resolution mass spectra (ESI-HRMS) were recorded on Bruker microTOF II an ESI-TOF Waters Micromass LCT spectrometer. Sample solutions of 50-100 ng/μL were prepared in CH_3CN. Calorimetric studies were conducted on a PerkinElmer DSC 8500. Variable temperature XRD (VT-XRD) measurements were performed on a Rigaku NANOPIX for liquid crystalline rotaxane via a thin glass capillary filled with argon gas. Other VT-XRD samples were prepared on a 2mm square aluminum pan and evaluated by a Rigaku XRD-DSC under nitrogen. XRD-DSC was equipped with a scintillation counter and operated at 40 kV and 40 mA. In both XRD studies, CuKα_1 radiation (λ = 1.54187 Å) was used. Optical polarized microscopy was performed on an Olympus BX53F2 with a METTLER TOLEDO HS82 hot-stage system. Polarized absorption spectra were collected with an IR spectrophotometer (JASCO, FT/IR-6100) equipped with a rotatable holder and a polarizer.

Compounds 4,4',5,5'-tetrabromomethyldibenzo[24]crown-8 ether (**S1**)[1], 4-(hexyloxy)phenol (**S2**, R = C6)[2], and 4-(dodecyloxy)phenol (**S2**, R = C12)[2] were synthesized following reported procedure; all spectroscopic characterization matched with the published data.

2. Synthesis

2.1. Synthesis scheme

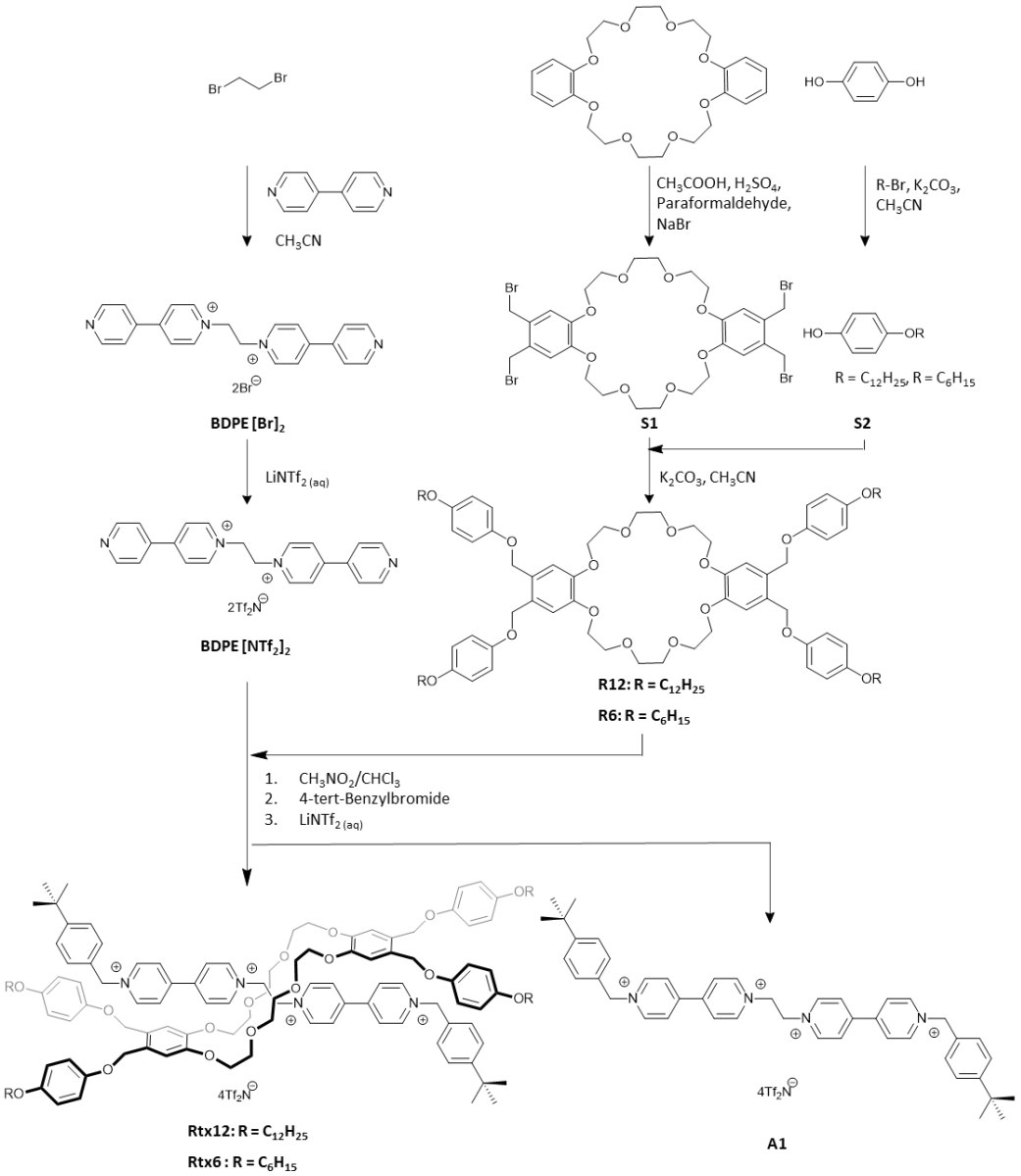

Scheme S1. Synthesis route to **Rtx12**, **Rtx6**, **R12**, **R6**, and **A1**.

2.2. Synthesis of $BDPE[NTf_2]_2$

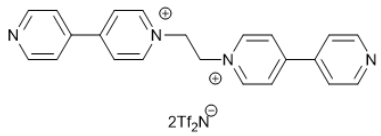

Figure S1. Chemical structure of $BDPE[NTf_2]_2$.

1,2-bis(4,4'-bipyridinium)ethane $(BDPE)[NTf_2]_2$ was synthesized by adapting the previously reported synthetic method[3]. 1,2-dibromoethane (0.96 g, 5.1 mmol) and 4,4'-dipyridyl (4.89 g, 31.3 mmol) were refluxed in 80 mL of acetonitrile at 80 °C for 24 h. After cooling the reaction to room temperature, the solid obtained by filtration was washed with acetonitrile (50 mL), ethanol (30 mL), and then chloroform (20 mL). After drying under reduced pressure, $BDPE[Br]_2$ was obtained as a light-yellow powder (0.83g, 1.7 mmol, 32% yield). Continuing with the ion exchange process, the obtained $BDPE[Br]_2$ was dissolved in water (20 mL) at 60 °C. A solution of lithium bis(trifluoromethane sulfonyl)imide ($LiNTf_2$) (2.0 g, 6.8 mmol) in 1 mL of water was added, and then the mixture was stirred at 60 °C for 0.5 h. After cooling to room temperature, the resulting suspension was filtered, and the collected solid was washed with water (3 × 15 mL), ethanol (3 × 10 mL), and chloroform (3 × 10 mL), followed by drying under reduced pressure to yield $BDPE[NTf_2]_2$ as a light-gray powder (1.4 g, 1.6 mmol, 93% yield). ^{1}H NMR (400 MHz, CD_3CN) δ = 8.90 (d, J = 6.1 Hz, 4H), 8.77 (d, J = 6.9 Hz, 4H), 8.43 (d, J = 6.9 Hz, 4H), 7.85 (d, J = 6.2 Hz, 4H), 5.19 (s, 4H). ^{13}C NMR (100 MHz, CD_3CN) δ = 155.8, 151.3, 145.5, 140.8, 126.8, 121.9, 59.4. ESI-HRMS: *m/z* calculated for $[BDPE]^{2+}$ C22H20N4, 170.0838; found, 170.0838; relative error 0.0 ppm.

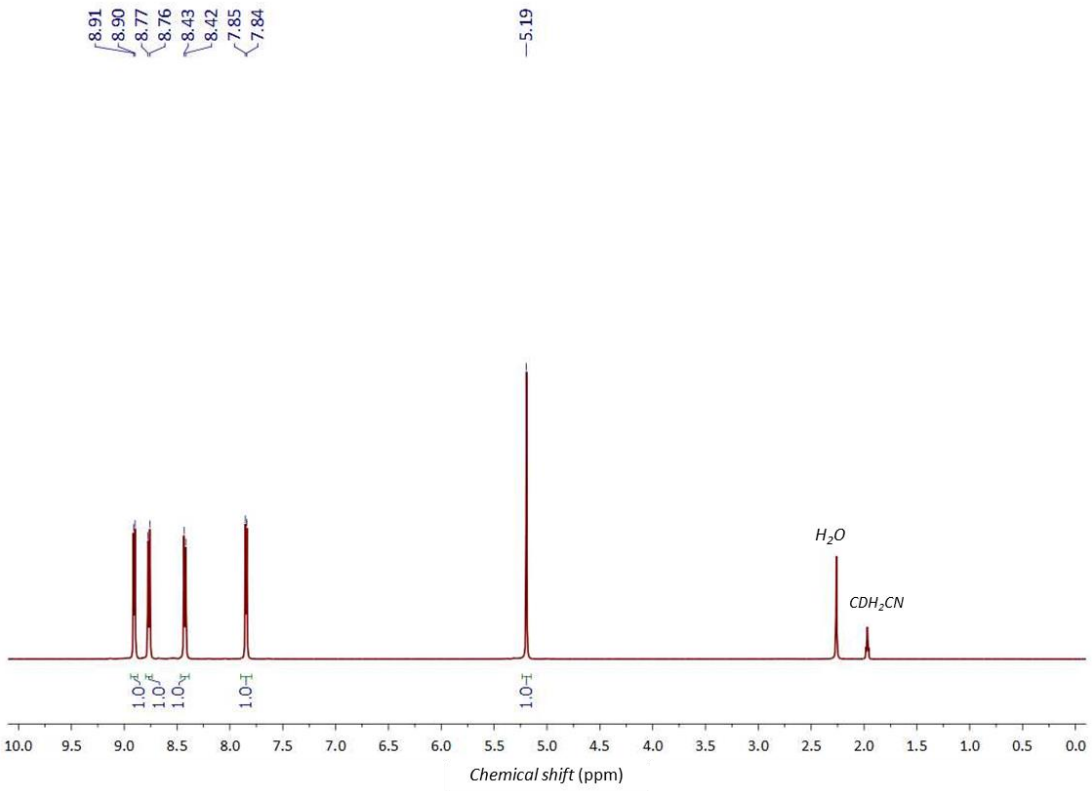

Figure S2. ^{1}H NMR spectrum (400 MHz, CD_3CN) of $BDPE[NTf_2]_2$.

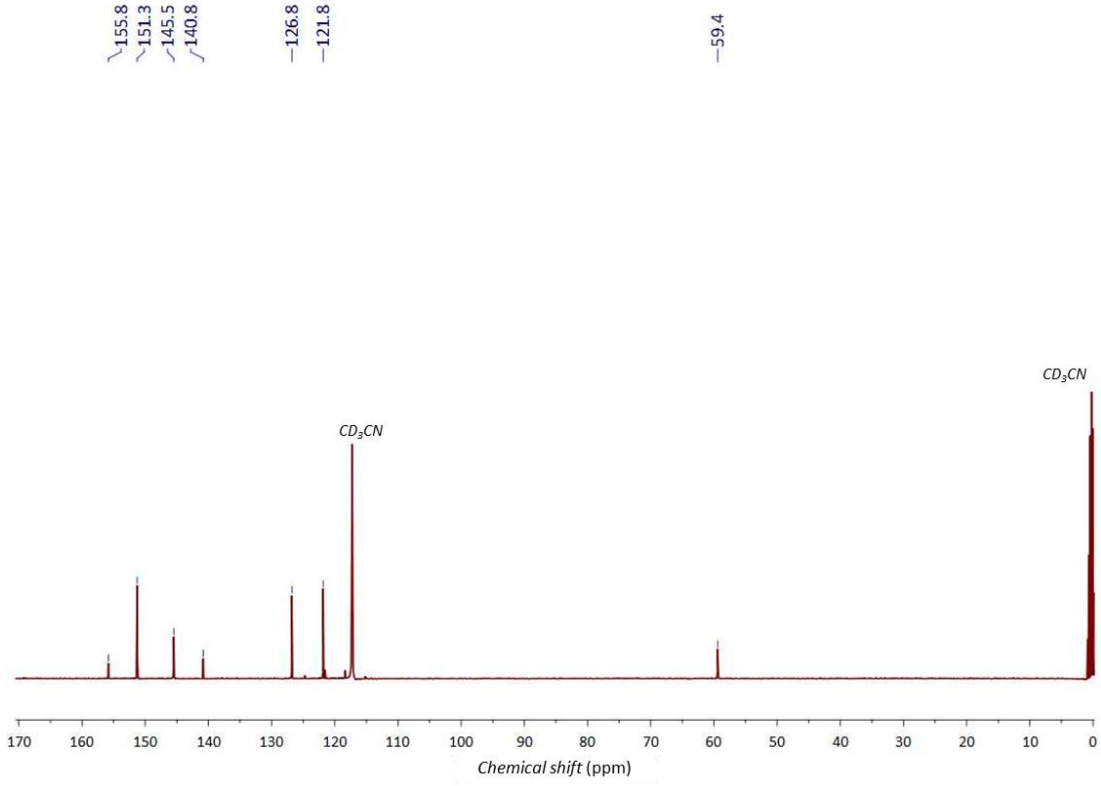

Figure S3. ^{13}C NMR spectrum (100 MHz, CD_3CN) of $BDPE[NTf_2]_2$.

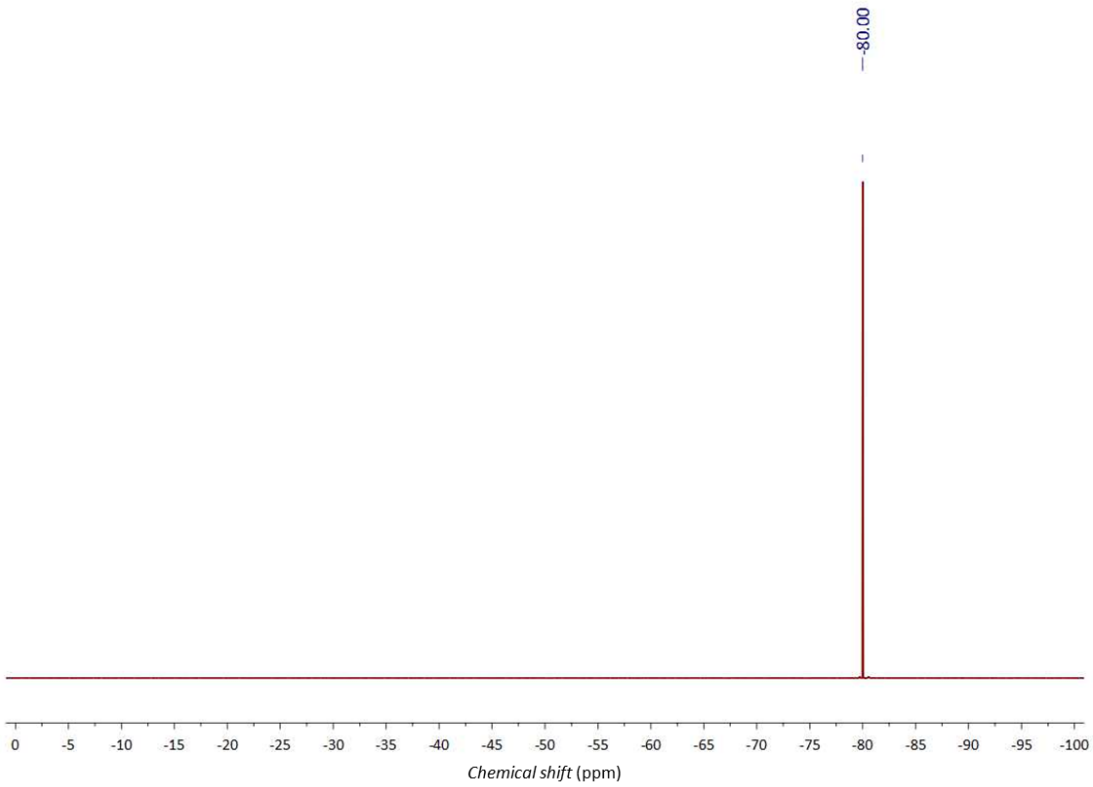

Figure S4. ^{19}F NMR spectrum (376 MHz, CD_3CN) of $BDPE[NTf_2]_2$.

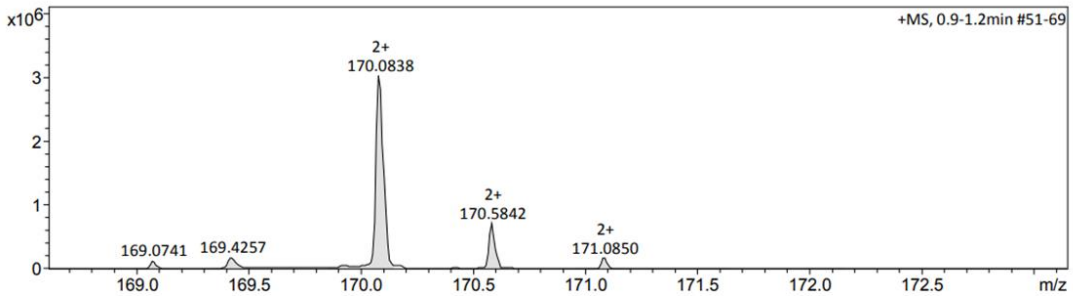

Figure S5. Partial ESI-HRMS of BDPE[NTf_2]$_2$.

2.3. Synthesis of **R12**

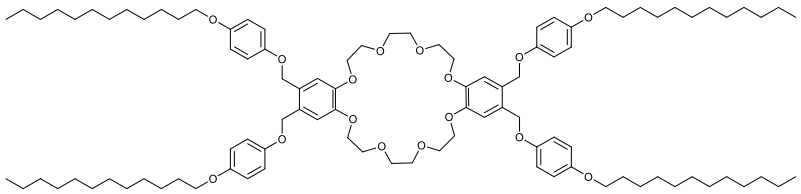

Figure S6. Chemical structure of **R12**.

Compound **S1**[1] (0.26 g, 0.32 mmol), 6 equivalents of compound **S2** (R=12)[2] (0.54 g, 1.9 mmol), and K_2CO_3 (1.1 g, 7.9 mmol) in dry acetonitrile (30 mL) were refluxed under a nitrogen atmosphere for 72 h. After cooling down to room temperature, the solid was filtered and then washed with chloroform (1 × 30 mL), which was combined with the filtrate. Evaporating all solvents under vacuum, the residue was dissolved in chloroform (50 mL), which was washed with water (2 × 40 mL) and then saturated brine (1 × 40 mL). The organic layer was dried over Na_2SO_4, followed by rotary evaporation. The crude product was purified by column chromatography (SiO_2, $CHCl_3$/MeOH (98:2), R_f = 0.30) affording **R12** as a white powder (0.36 g, 0.22 mmol, yield 69%). ^{1}H NMR (400 MHz, $CDCl_3$) δ (ppm) = 7.02 (s, 4H), 6.85 (dd, *J* = 9.1 Hz, 16H), 5.00 (s, 8H), 4.18 (t, *J* = 4.1 Hz, 8H), 3.91 (m, 16H), 3.84 (m, 8H), 1.76 (quin, *J* = 7.0 Hz, 8H), 1.46 (m, 8H), 1.29 (br, 64H), 0.90 (t, *J* = 6.8 Hz, 12H). ^{13}C NMR (100 MHz, $CDCl_3$) δ = 153.6, 152.7, 148.6, 128.5, 115. 9, 115.4, 115.1, 71.3, 69.9, 69.6, 68.6, 68.4, 31.8, 29.4, 29.3, 26.1, 22.7, 14.1. ESI-HRMS: *m/z* calculated for [**R12** + Na]$^+$ C100H152NaO16, 1633.0995; found, 1633.0995; relative error −0.7 ppm.

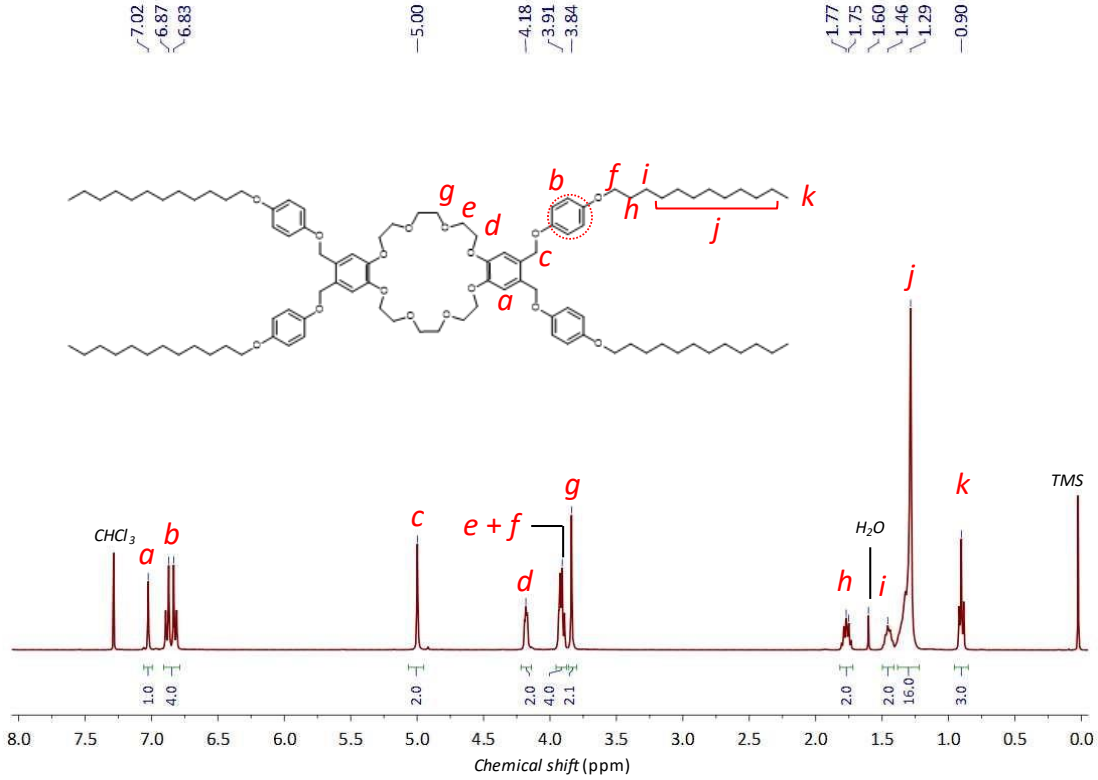

Figure S7. ^{1}H NMR spectrum (400 MHz, $CDCl_3$) of **R12**.

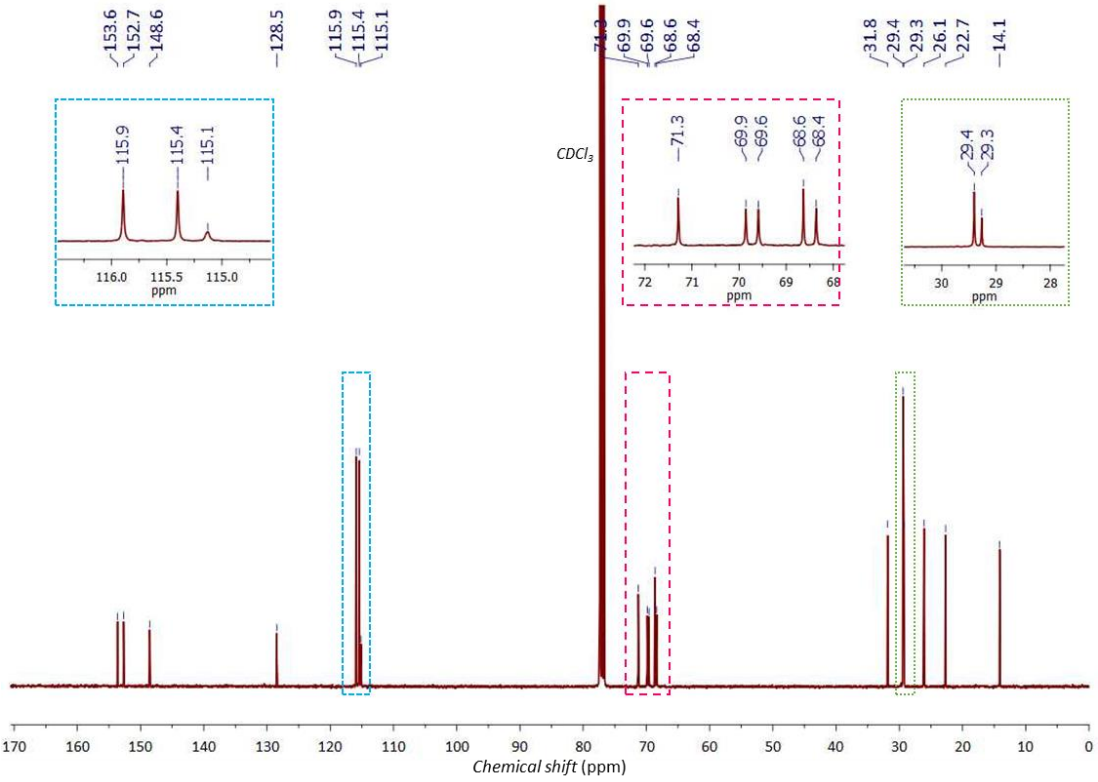

Figure S8. ^{13}C NMR spectrum (100 MHz, $CDCl_3$) of **R12**.

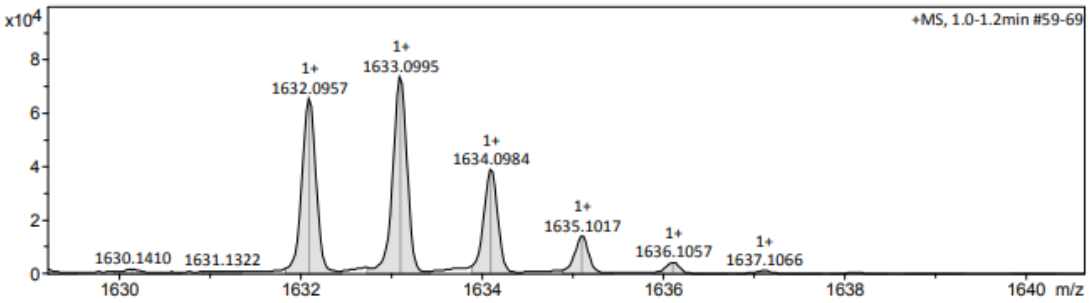

Figure S9. Partial ESI-HRMS of **R12**.

2.4. Synthesis of **R6**

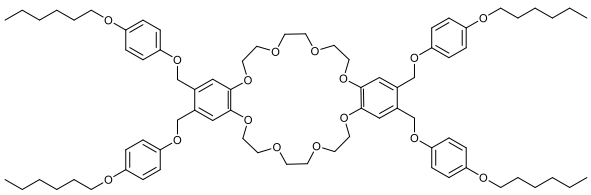

Figure S10. Chemical structure of **R6**.

Compound **S1**[1] (0.40 g, 0.49 mmol), 4.8 equivalents of compound **S2** (R = 6)[2] (0.46 g, 2.4 mmol), and K_2CO_3 (1.1 g, 8.5 mmol) in dry acetonitrile (30 mL) were refluxed under a nitrogen atmosphere for 72 h. After cooling down to room temperature, the solid was filtered out collecting the filtrate, and the removed solid was extracted with chloroform (1 × 30 mL). After combining all solutions followed by evaporating all solvents under vacuum, the residue was dissolved in chloroform (50 mL), followed by washing with water (2 × 40 mL) and then saturated brine (1 × 40 mL). The organic layer was dried over Na_2SO_4, and then the solvent was removed by rotary evaporation. Column chromatography of the crude compound (SiO_2, CH_3CN/EtOAc (8:2), R_f = 0.21) yielded **R6** as a white powder (0.58 g, 0.46 mmol, 93% yield). ^{1}H NMR (400 MHz, $CDCl_3$) δ = 7.02 (s, 4H), 6.85 (dd, J = 9.1 Hz, 16H), 5.00 (s, 8H), 4.18 (t, J = 4.2 Hz, 8H), 3.91 (m, 16H), 3.83 (m, 8H), 1.77 (quin, J = 7.1 Hz, 8H), 1.46 (quin, J = 7.2 Hz, 8H), 1.35 (m, 16H), 0.92 (t, J = 6.9 Hz, 12H). ^{13}C NMR (100 MHz, $CDCl_3$) δ = 153.7, 152.8, 148.7, 128.6, 116.0, 115.5, 115.4, 71.3, 69.9, 69.7, 68.7, 68.5, 31.6, 29.4, 25.7, 22.6, 14.0. ESI-MRMS: *m/z* calculated for [**R6** + Na]$^+$ C76H104NaO16, 1295.7217; found, 1295.7213; relative error −0.3 ppm.

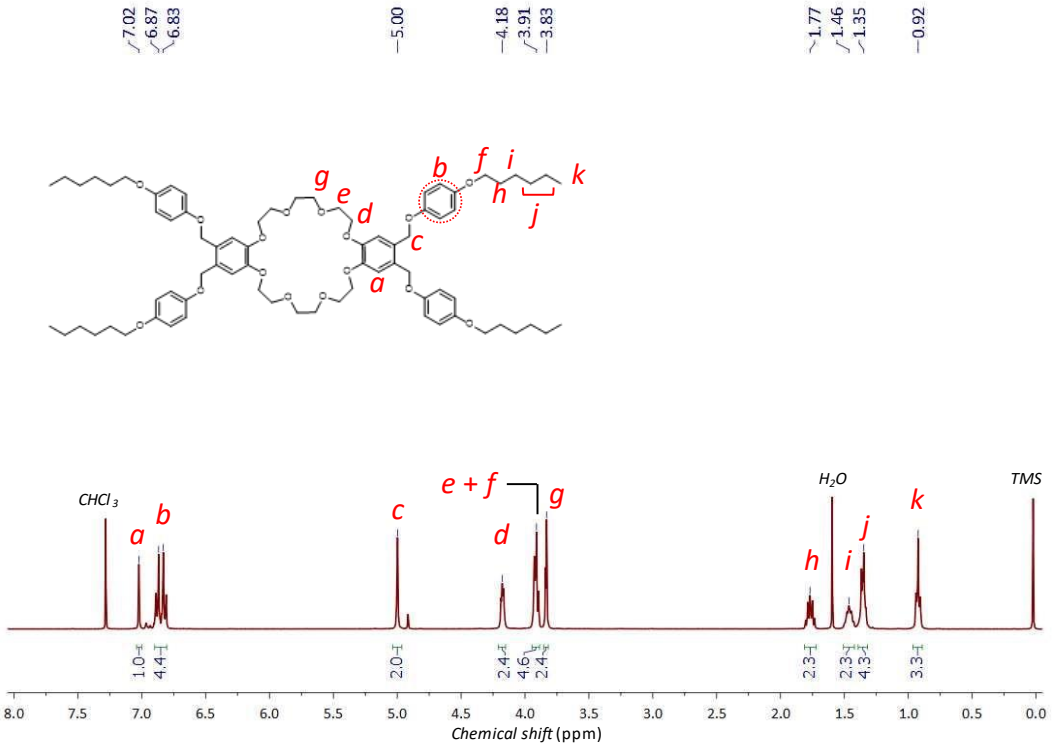

Figure S11. ^{1}H NMR spectrum (400 MHz, $CDCl_3$) of **R6**.

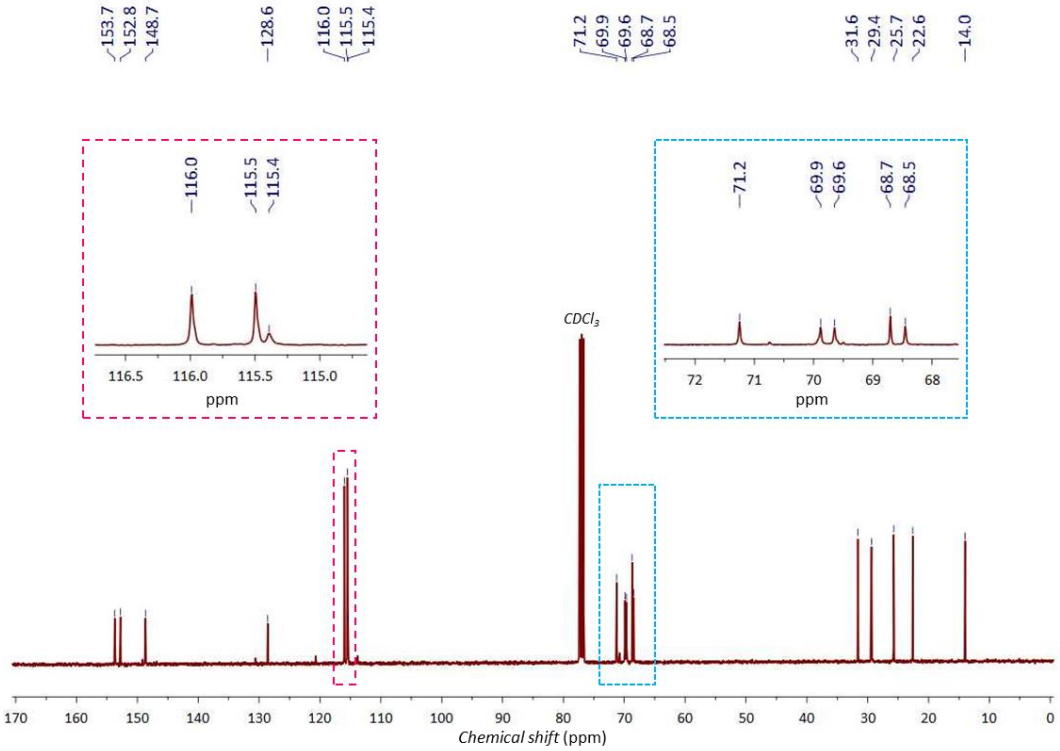

Figure S12. ^{13}C NMR spectrum (100 MHz, $CDCl_3$) of **R6**.

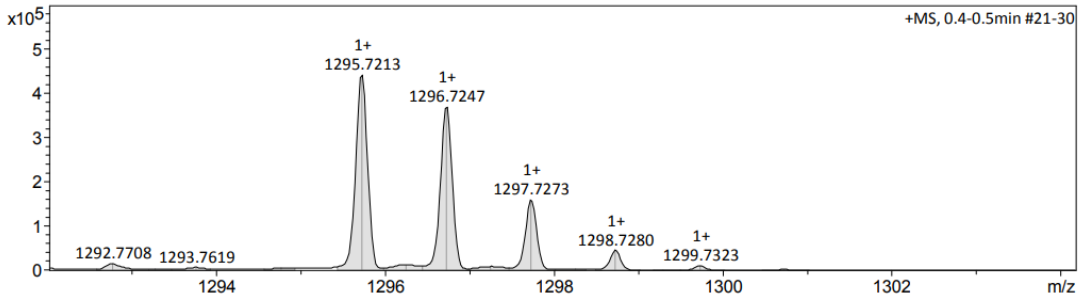

Figure S13. Partial ESI-HRMS of **R6**.

2.5. Synthesis of **Rtx0**

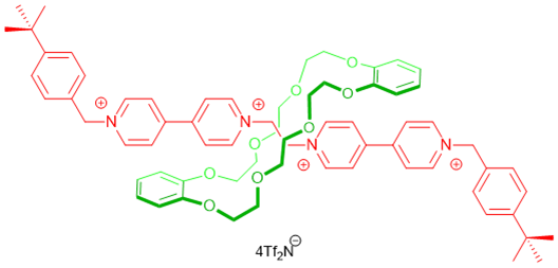

Figure S14. Chemical structure of **Rtx0**.

Rtx0 was synthesized according to the previously reported procedure[4]. The addition of dibenzo-24-crown-8 (DB24C8) (0.10 g, 0.23 mmol) to a solution of BDPE[NTf_2] (0.14 g, 0.15 mmol) in $MeNO_2$/$CHCl_3$ (3.5 mL, 4:3, v/v) caused the solution to exhibit deep yellow. After stirring for 10 min, 4-*tert*-benzyl bromide (0.53 mL, 2.9 mmol) and 0.3 mL of aqueous solutions of $LiNTf_2$ (0.28 g, 0.97 mmol) were added to the reaction with a pipette, respectively, followed by stirring for 4 days at room temperature. The reaction solution was washed with water (3 × 10 mL), dried over Na_2SO_4, and then all organic solvents were removed with a rotary evaporator. The obtained crude product was isolated by column chromatography (SiO_2, CH_3CN/MeOH/2M NH_4Cl (aq) (60/28/12), R_f = 0.25), and all organic solvents of the collected fractions were evaporated under vacuum. To the residue, 4 mL of MeOH was added to make a homogeneous solution, then the solution was suspended by adding an excess amount of $LiNTf_2$ (0.22 g) in 0.3 mL of water. The solid was collected by filtration, washed with water and MeOH (2 × 10 mL, each), and dried under reduced pressure yielding **Rtx0** as an orange solid (100 mg, 46 μmol, 30% yield). ^{1}H NMR (400 MHz, $CDCl_3$) δ = 9.30 (d, J = 6.9 Hz, 2H), 8.93 (d, J = 6.9 Hz, 4H), 8.12 (d, J = 6.9 Hz, 4H), 8.07 (d, J = 6.8 Hz, 4H), 7.59 (d, J = 8.4 Hz, 4H), 7.47 (d, J = 8.4 Hz, 4H), 6.64 (dd, J = 6.0, 3.6 Hz, 4H), 6.45 (dd, J = 6.0, 3.5 Hz, 4H), 5.81 (s, 4H), 5.60 (s, 4H), 4.08–3.95 (m, 24H), 1.34 (s, 18H). ESI-HRMS: *m/z* calculated for [**Rtx0** + $(NTf_2)_2]^{2+}$ C72H82F12N6O16S4, 821.2234; found, 821.22242; relative error 0.9 ppm.

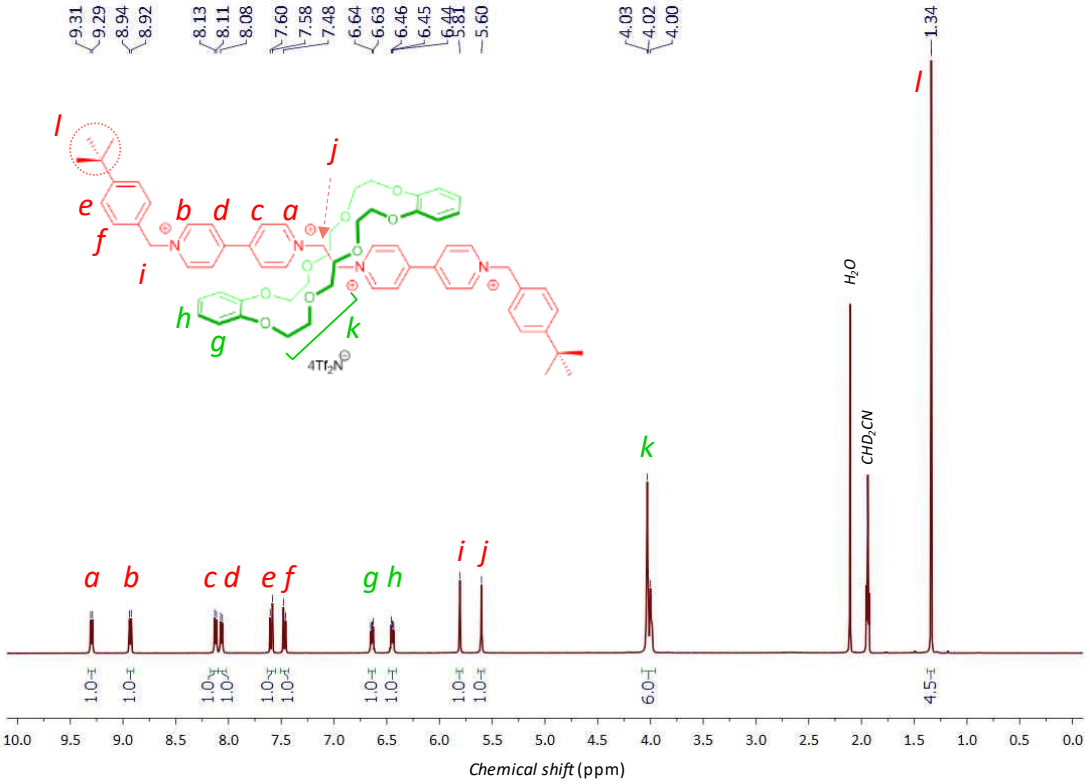

Figure S15. ^{1}H NMR spectrum (400 MHz, CD_3CN) of **Rtx0**.

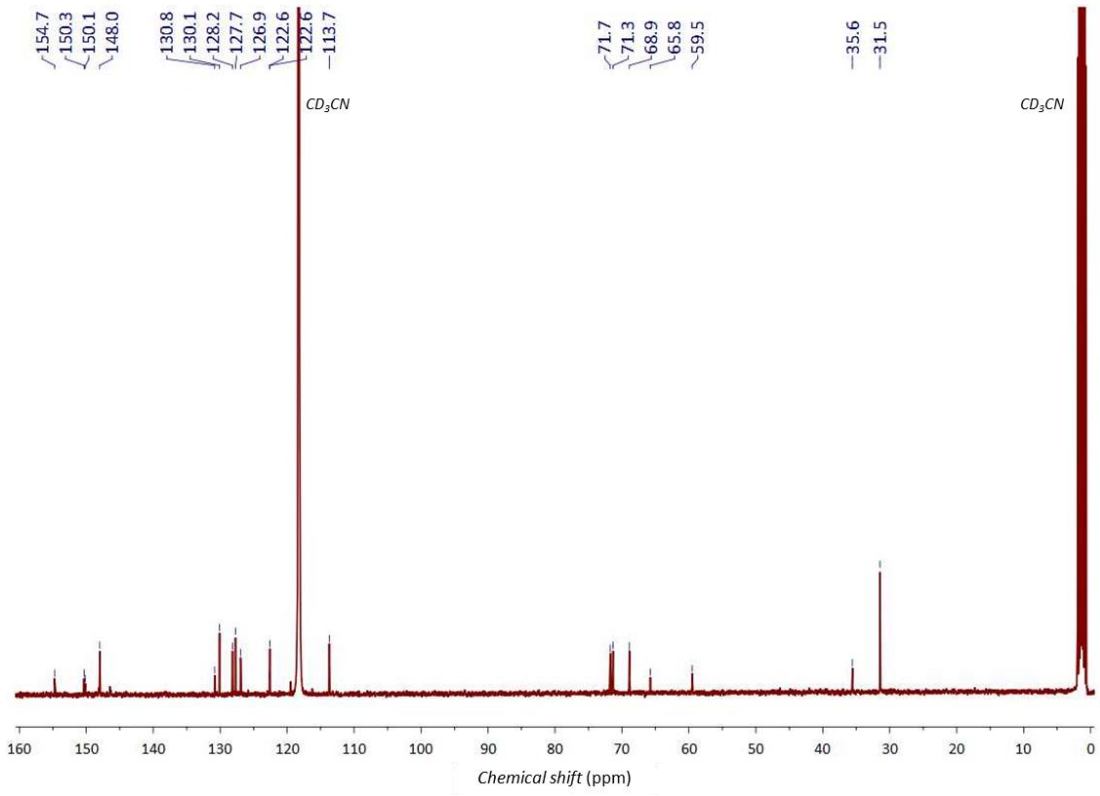

Figure S16. ^{13}C NMR spectrum (100 MHz, CD_3CN) of **Rtx0**.

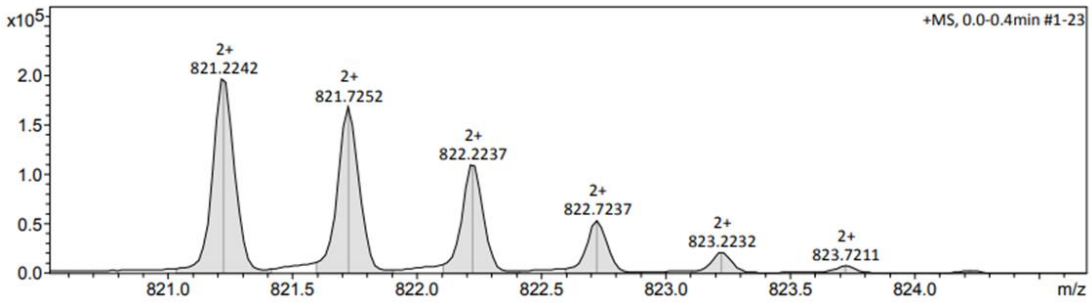

Figure S17. Partial ESI-HRMS of **Rtx0**.

2.6. Synthesis of **Rtx12**

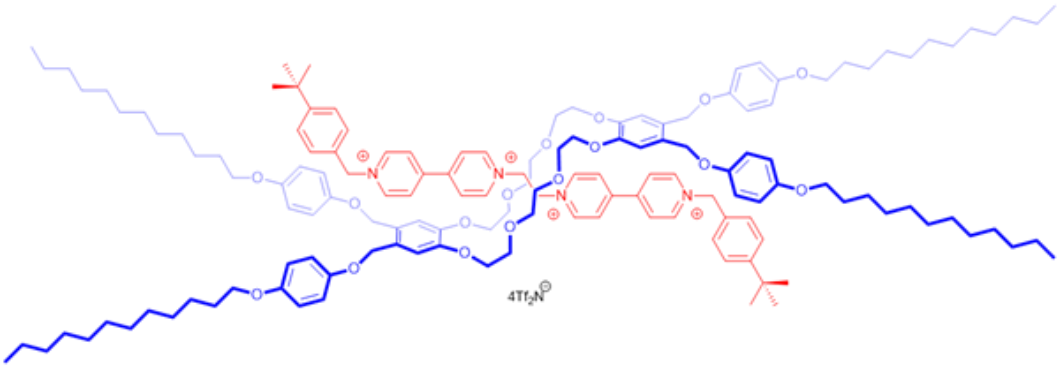

Figure S18. Chemical structure of **Rtx12**.

Rtx12 was synthesized according to the procedure for **Rtx0**. A dark orange solution obtained by mixing a solution of BDPE[NTf_2]$_2$ (0.11 g, 0.13 mmol) in 2 mL of $MeNO_2$ with a solution of **R12** (0.13 g, 0.08 mmol) in 1 mL of $CHCl_3$ was stirred at room temperature for 0.5 h. To this reaction, 4-*tert*-benzyl bromide (0.14 mL, 0.75 mmol) and a solution of $LiNTf_2$ (0.29 g, 1.0 mmol) in 0.3 mL water were added with a pipette, and then the reaction was stirred at room temperature for another 5 days. After adding 10 mL of $MeNO_2$, the reaction was washed with water (3 × 10 mL), and dried over $MgSO_4$, followed by rotary evaporation to remove all organic solvents. The addition of $CHCl_3$ (20 mL) to the remaining solid affords a suspension. The emerging solid (**A1**, see Section 2.7) was filtered off, followed by washing with $CHCl_3$ till the wash solution became colorless. The filtrate and the wash solution were combined and then evaporated. The obtained crude product was purified by column chromatography (SiO_2, CH_3CN/ MeOH/2M NH_4Cl (aq) (60/38/2), R_f = 0.27). All organic solvents of the collected fractions were removed under vacuum, and then 20 mL of MeOH was added. An excess amount of $LiNTf_2$ (0.6 g) in 1.5 mL MeOH was added to the obtained solution to ensure the exchange of the counter anion to NTf_2^-, which afforded a suspension. The emerged solid was collected by filtration, washed with MeOH (2 × 10 mL), and then dried under reduced pressure to yield **Rtx12** (21 mg, 6.4 µmmol, 8% yield) as an orange solid. ^{1}H NMR (400 MHz, CD_3CN) δ = 9.37 (d, J = 6.7 Hz, 4H), 8.78 (d, J = 6.8 Hz, 4H), 8.19 (d, J = 6.7 Hz, 4H), 8.13 (d, J = 6.8 Hz, 4H), 7.39 (d, J = 8.4 Hz, 4H), 7.22 (d, J = 8.4 Hz, 4H), 6.91-6.83 (m, 20H), 5.63 (s, 4H), 5.52 (s, 4H), 4.63 (s, 8H), 4.08 (br, 24H), 3.97 (t, J = 6.5 Hz, 8H), 1.76 (quin, J = 7.0Hz, 8H), 1.47-1.27 (m, 136H), 0.91 (t, J = 6.8 Hz, 12H). ^{13}C NMR (100 MHz, CD_3CN) δ = 153.9, 153.5, 152.4, 149.3, 147.3, 146.5, 145.1, 129.3, 128.9, 128.4, 127.1, 126.6, 126.0, 121.5, 118.4, 116.0, 115.6, 115.3, 113.8, 70.6, 70.1, 68.4, 68.0, 67.7, 64.3, 58.5, 34.4, 31.7, 30.4, 29.3, 29.1, 29.1, 29.1, 25.8, 22.4, 13.4. ESI-HRMS: *m/z* calculated for [**Rtx12** + $(NTf_2)_2$]$^{2+}$ $C_{148}H_{202}F_{12}N_6O_{24}S_4$, 1402.1760; found, 1402.1742; relative error −1.2 ppm.

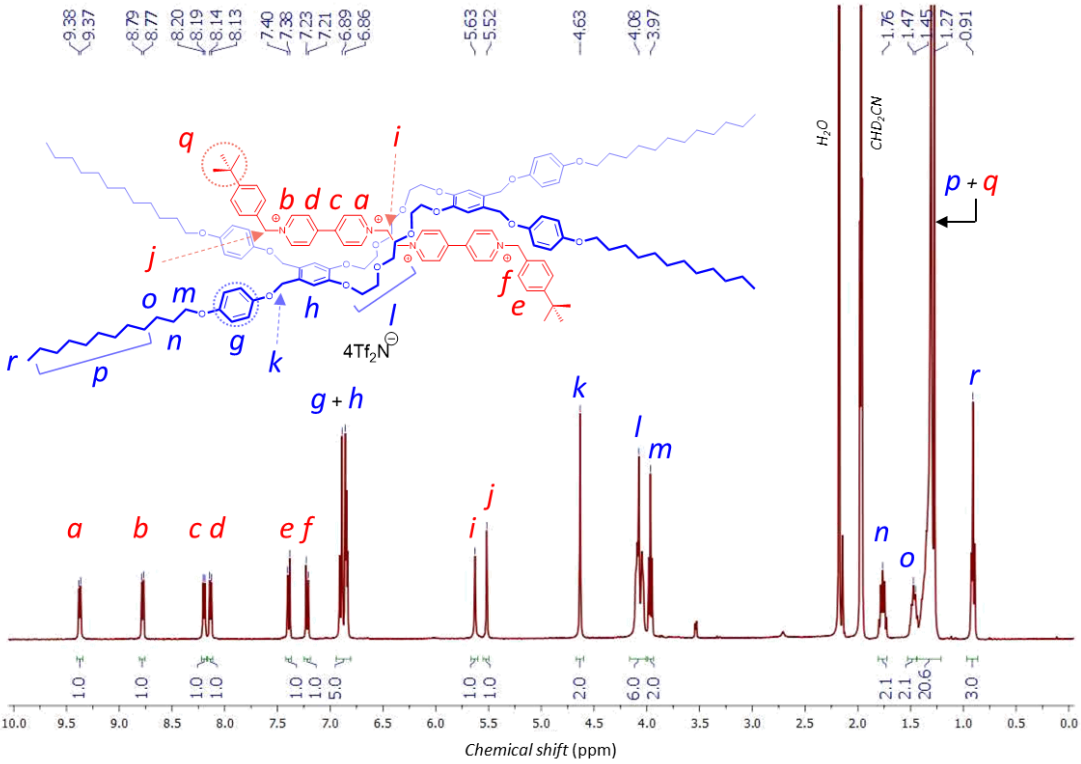

Figure S19. ^{1}H NMR spectrum (400 MHz, CD_3CN) of **Rtx12**.

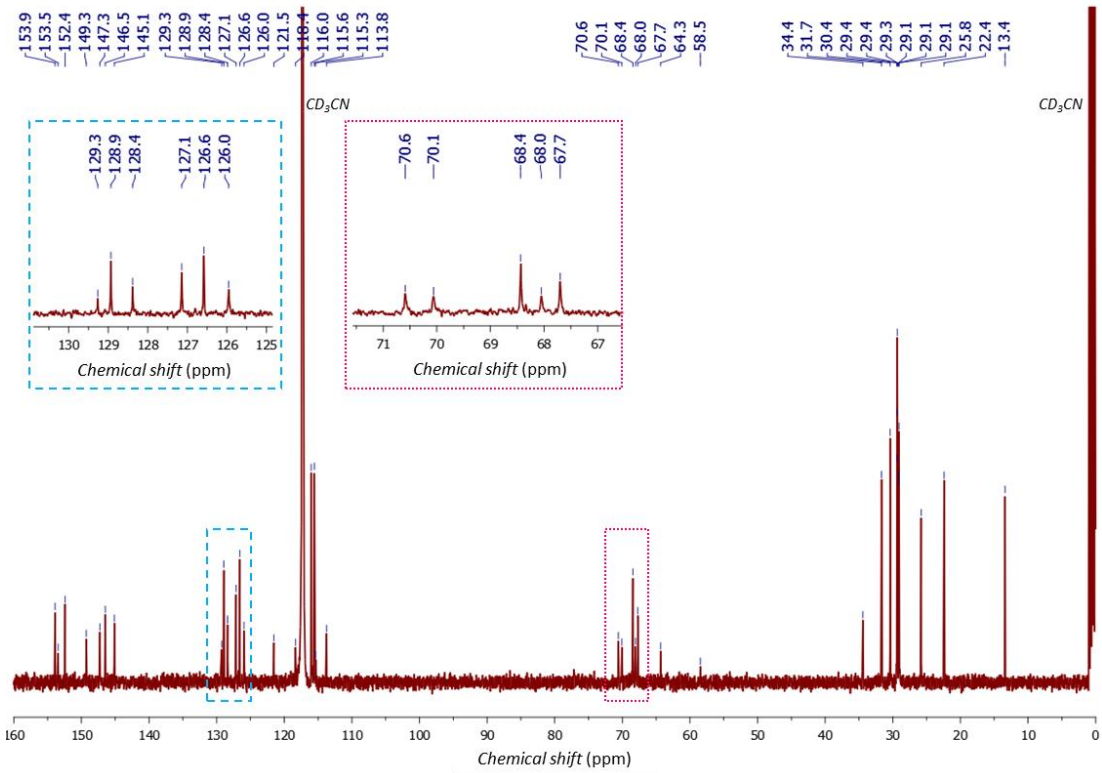

Figure S20. ^{13}C NMR spectrum (100 MHz, CD_3CN) of **Rtx12**.

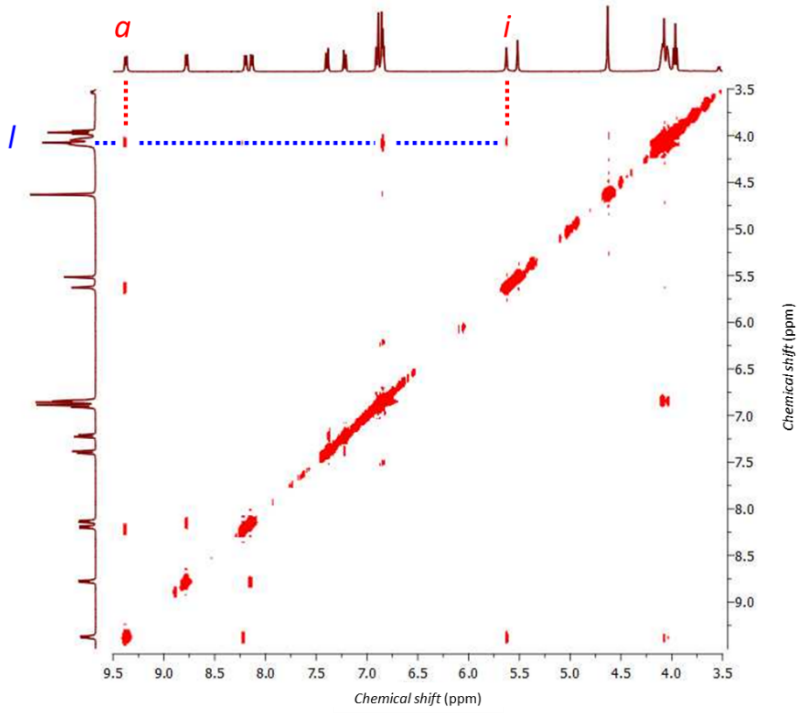

Figure S21. ^{1}H-^{1}H NOESY NMR spectrum (400 MHz, CD_3CN) of **Rtx12**; dash lines indicate correlations.

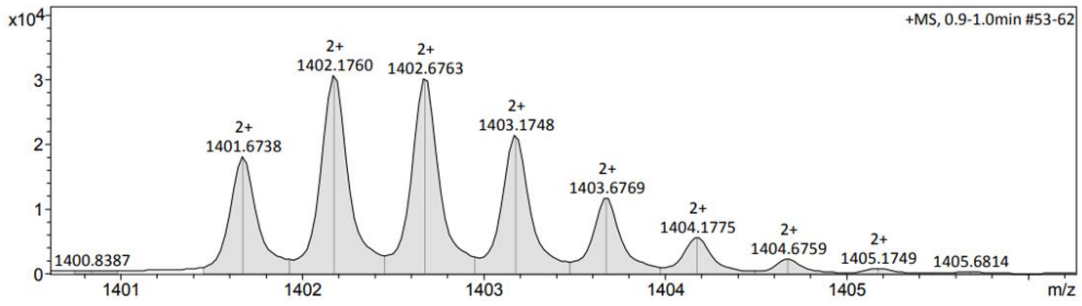

Figure S22. Partial ESI-HRMS of **Rtx12**.

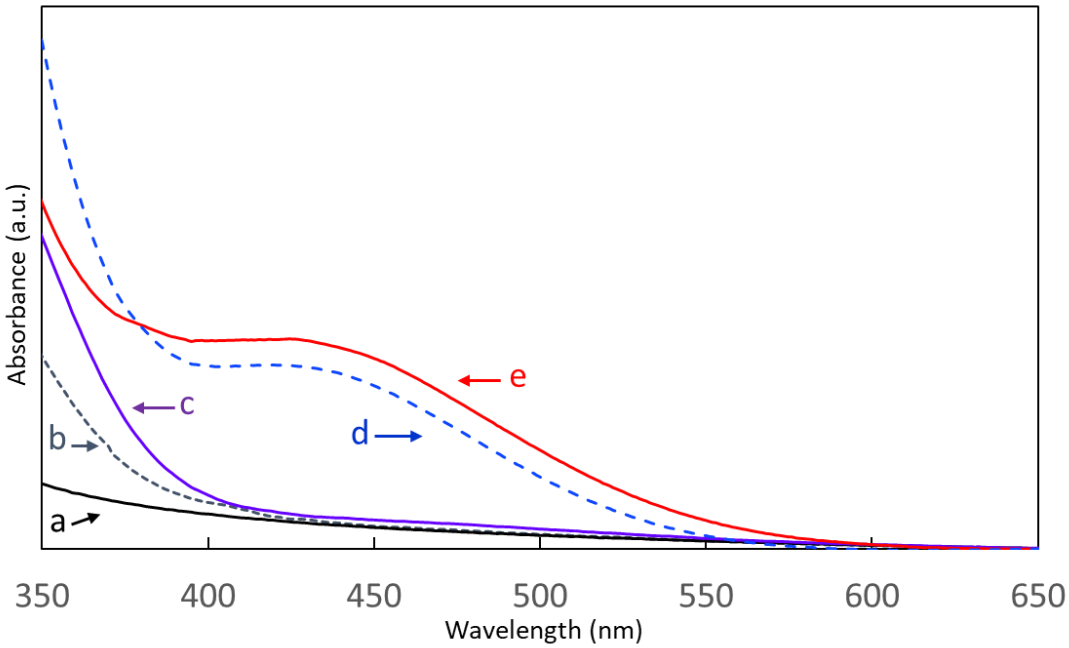

Figure S23. UV-vis spectrum of a) **R12**, b) **A1**, c) 1:1 mixture of **A1** and **R12**, d) **Rtx0**, and e) **Rtx12**; samples were prepared in films sandwiched between two glass slides.

Table S1. A comparison of ^{1}H NMR chemical shifts derived from **A1** in each state of bare **A1**, **Rtx12**, and **Rtx0**. All spectra were collected in CD_3CN at 24 °C. The assigned proton labels are found in **Figure S28**. The results of bare **A1** and **A1** in **Rtx0** were in good agreement with those reported by Mercer[4]. The chemical shifts observed in **Rtx12** were identical to those in **Rtx0**, supporting that **Rtx12** has the [2]rotaxane structure where **A1** threads a DB24C8 derivative ring.

δ ($\Delta\delta$) values in ppm			
proton	Bare **A1**	In **Rtx12** (**A1** ⊂ **R12**)	In **Rtx0** (**A1** ⊂ **DB24C8**)
a	9.03	9.37 (+0.34)	9.30 (+0.27)
b	8.95	8.78 (−0.17)	8.93 (−0.02)
c	8.50	8.19 (−0.30)	8.12 (−0.37)
d	8.43	8.13 (−0.29)	8.07 (−0.35)
e	7.58	7.39 (−0.19)	7.59 (+0.01)
f	7.49	7.22 (−0.26)	7.47 (−0.01)
g	5.84	5.52 (−0.31)	5.81 (−0.02)
h	5.25	5.63 (+0.40)	5.60 (+0.37)
i	1.35	1.27 (−0.08)	1.34 (−0.01)

2.7. Synthesis of **Rtx6**

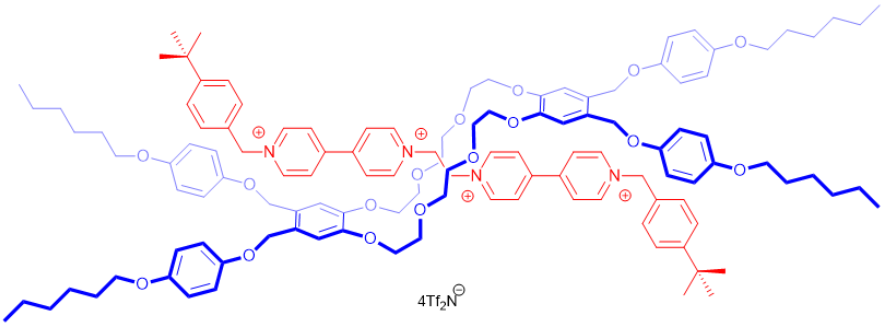

Figure S24. Chemical structure of **Rtx6**.

Rtx6 was prepared by the identical synthetic procedure to **Rtx12**. The addition of BDPE[NTf_2]$_2$ (0.44 g, 0.49 mmol) to a solution of **R6** (0.21 g, 0.16 mmol) in $MeNO_2$/$CHCl_3$ (3 mL, 2:1, v/v) produced a dark orange solution, which was stirred at room temperature for 0.5 h. After adding 4-*tert*-benzyl bromide (0.53 mL, 2.9 mmol) and 0.5 mL of an aqueous solution of $LiNTf_2$ (0.57 g, 1.9 mmol) with a pipette, the reaction was stirred at room temperature for 5 days. $MeNO_2$ (10 mL) was added to the reaction, washed with water (3 × 10 mL), dried over $MgSO_4$, and then all organic solvents were evaporated. To the residue, $CHCl_3$ (10 mL) was added to precipitate byproduct, solid **A1**, which was filtered off, and then the collected solution was evaporated under vacuum. The obtained crude product was purified by column chromatography (SiO_2, CH_3CN/CH_3OH/2M NH_4Cl (aq) (60/38/2), R_f = 0.30). All organic solvents of the collected fractions were removed with a rotary evaporator, and a solution of $LiNTf_2$ (1 g) in water (3 mL) was added to the residue. The precipitated solid was filtered and dried under reduced pressure to yield an orange solid of **Rtx6** (23 mg, 7.7 µmol, 5% yield). ^{1}H NMR (400 MHz, CD_3CN) δ = 9.39 (d, J = 6.8 Hz, 4H), 8.79 (d, J = 6.9 Hz, 4H), 8.20 (d, J = 6.8 Hz, 4H), 8.13 (d, J = 6.8 Hz, 4H), 7.41 (d, J = 8.4 Hz, 4H), 7.23 (d, J = 8.4 Hz, 4H), 6.92-6.85 (m, 20H), 5.66 (s, 4H), 5.53 (s, 4H), 4.66 (s, 8H), 4.09 (br, 24H), 3.98 (t, J = 6.5 Hz, 8H), 1.77 (quin, J = 7.0 Hz, 8H), 1.49 (br, 8H), 1.40-1.36 (m, 16H), 1.28 (br, 18H), 0.94 (t, J = 7.1Hz, 12H). ^{13}C NMR (100 MHz, CD_3CN) δ = 154.0, 153.6, 152.5, 149.4, 149.3, 147.3, 146.6, 145.1, 129.2, 128.9, 128.5, 127.1, 126.6, 125.9, 121.6, 118.4, 116.1, 115.6, 113.8, 70.6, 70.1, 68.5, 67.8, 64.4, 58.5, 34.4, 31.3, 30.4, 29.1, 25.5, 22.3, 13.3. ESI-HRMS: *m/z* calculated for [**Rtx6** + $(NTf_2)_2$]$^{2+}$ C124H154F12N6O24S4, 1233.9863; found, 1233.9871; relative error −0.6 ppm.

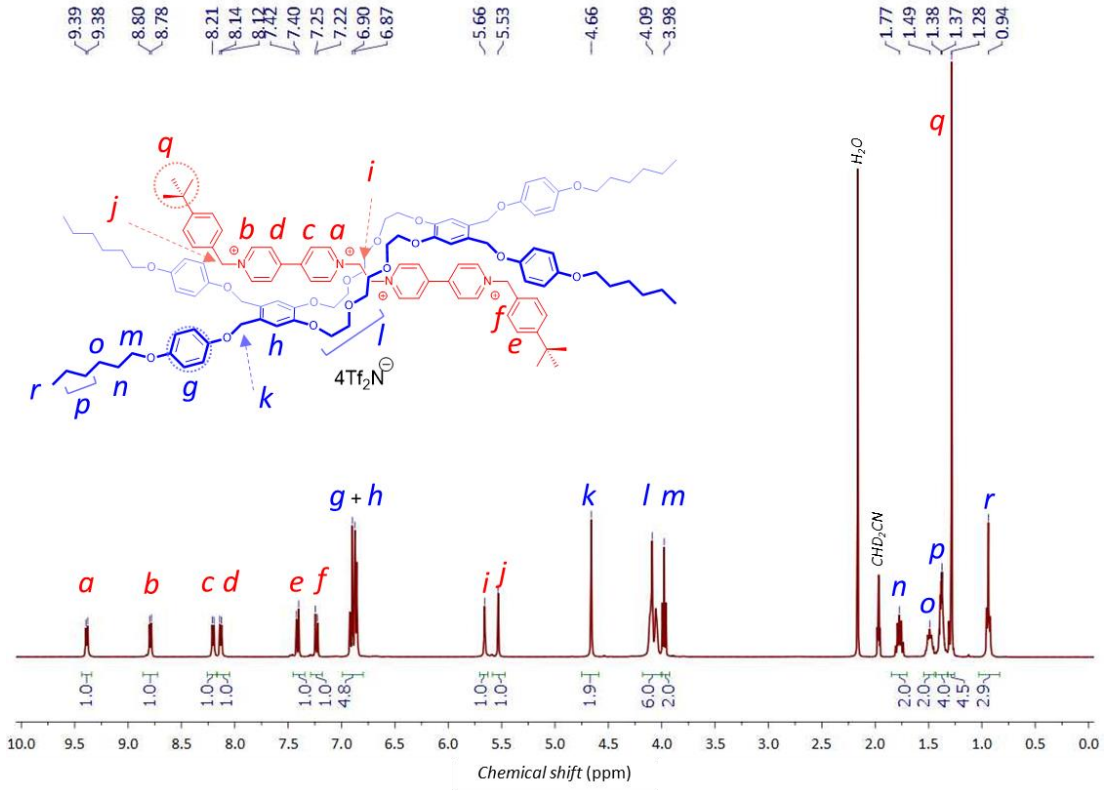

Figure S25. ^{1}H NMR spectrum (400 MHz, CD_3CN) of **Rtx6**.

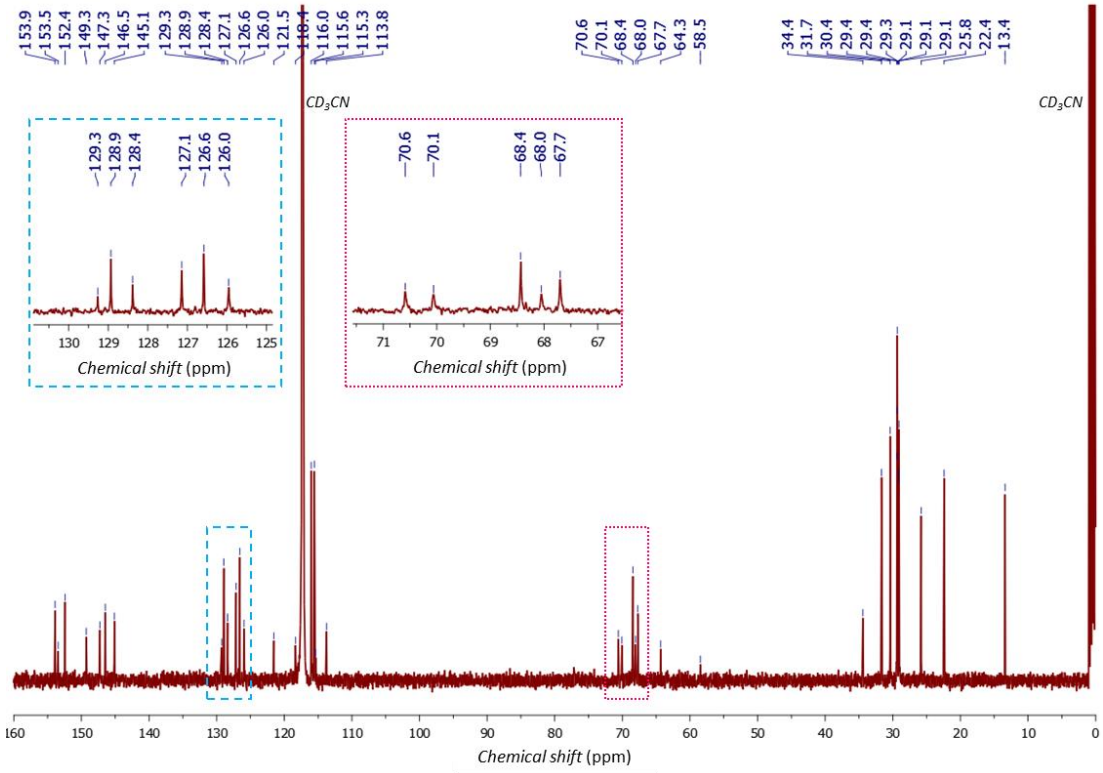

Figure S26. ^{13}C NMR spectrum (100 MHz, CD_3CN) of **Rtx6**.

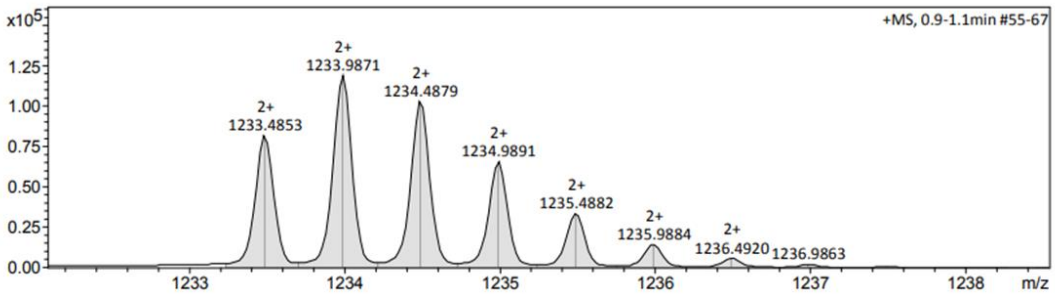

Figure S27. Partial ESI-HRMS of **Rtx6**.

2.8. Synthesis of **A1**$[NTf_2]_2$

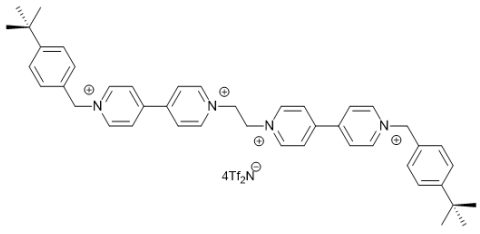

Figure S28. Chemical structure of **A1**$[NTf_2]_2$.

A1[NTf_2]$_2$ was yielded as a byproduct in the synthesis of **Rtx12**. A solution of BDPE[NTf_2]$_2$ (0.11 g, 0.13 mmol) and **R12** (0.13 g, 0.08 mmol) in a mixed solvent of $MeNO_2$ and $CHCl_3$ (3 mL, 2:1, v/v) was stirred at room temperature for 5 days, washed with water (3 × 20 mL), and dried over $MgSO_4$, and then all solvents were removed under vacuum. Chloroform (10 mL) was added to the crude product, and the resulting solid was filtered off followed by further washing with $CHCl_3$ (3 × 10 mL) to afford **A1**[NTf_2]$_2$ (0.18 g, 0.9 mmol, 81% yield). ^{1}H NMR (400 MHz, CD_3CN) δ = 9.03 (d, J = 6.7 Hz, 4H), 8.95 (d, J = 6.7 Hz, 4H), 8.50 (d, J = 6.7 Hz, 4H), 8.43 (d, J = 6.6 Hz, 4H), 7.58 (d, J = 8.3 Hz, 4H), 7.49 (d, J = 8.3 Hz, 4H), 5.84 (s, 4H), 5.25 (s, 2H), 1.35 (s, 18H). ^{13}C NMR (100 MHz, CD_3CN) δ = 153.5, 151.5, 149.9, 146.3, 145.6, 129.6, 129.1, 128.0, 127.6, 126.6, 121.5, 118.3, 64.7, 59.6, 34.5, 30.4. ESI-HRMS: *m/z* calculated for [**A1** + $(NTf_2)_2$]$^{2+}$ C48H50F12N6O8S4, 597.1185; found, 597.1194; relative error 1.5 ppm.

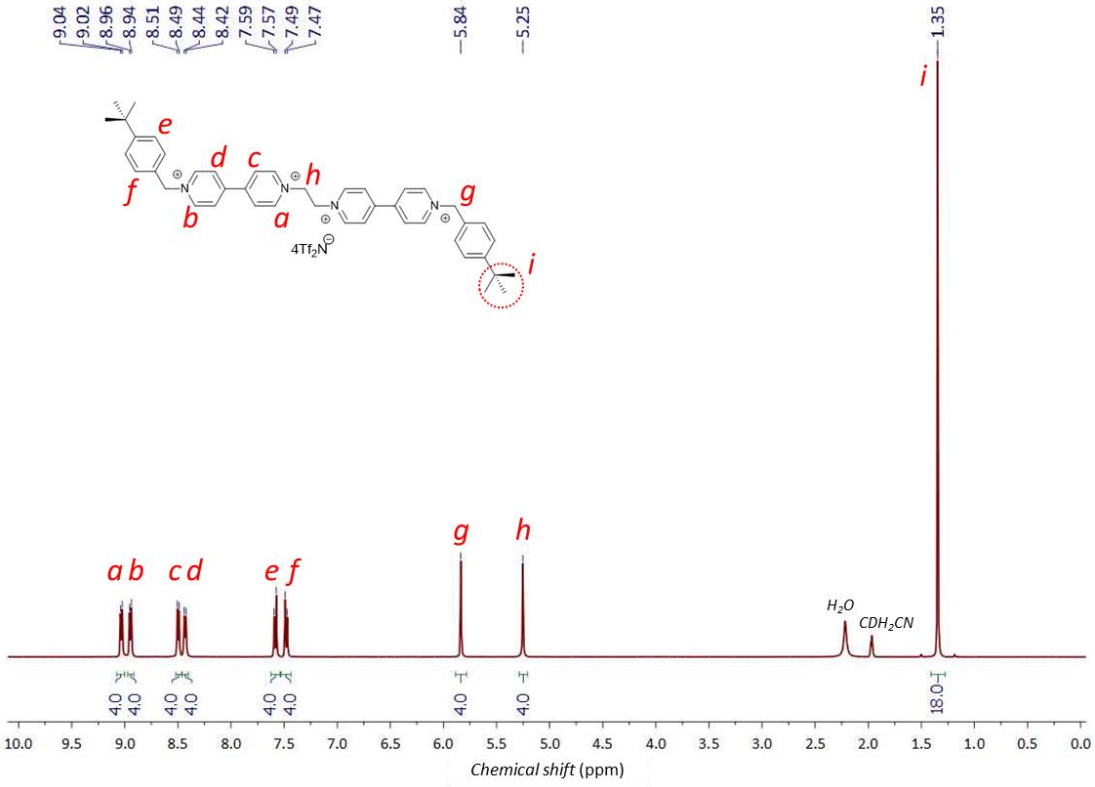

Figure S29. ^{1}H NMR spectrum (400 MHz, CD_3CN) of **A1**.

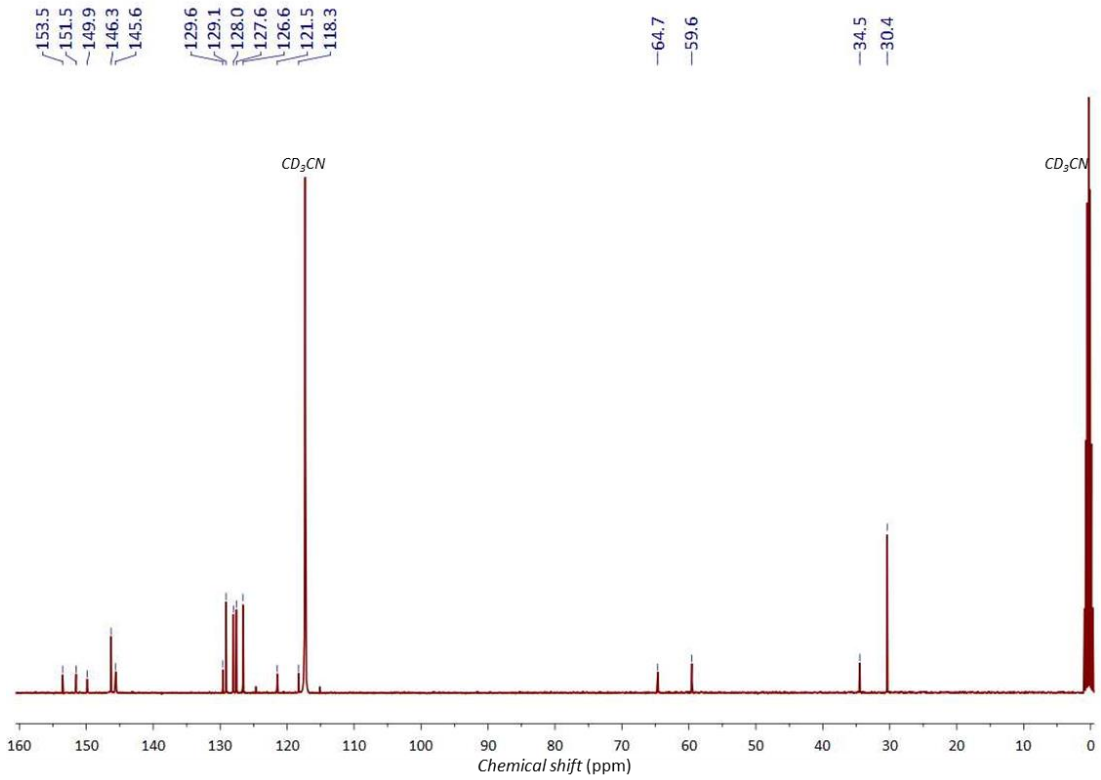

Figure S30. ^{13}C NMR spectrum (100 MHz, CD_3CN) of **A1**.

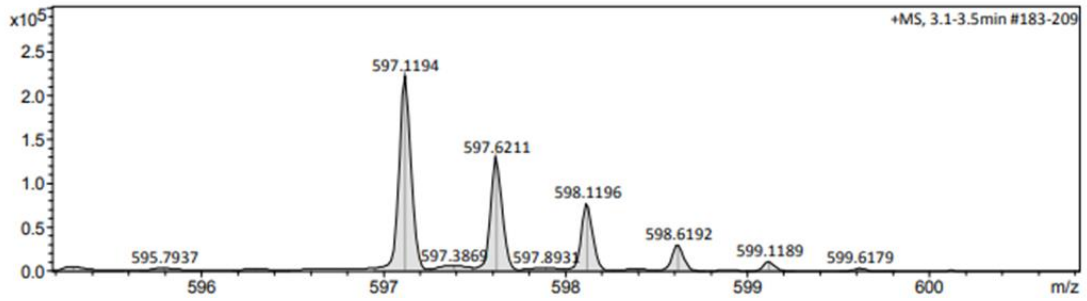

Figure S31. Partial ESI-HRMS of **A1**.

3. Thermodynamic and Structural Studies of Rtx12

3.1. Thermodynamic studies of **Rtx12**

As reported in the main manuscript, **Rtx12** stably showed a smectic A phase in the cooling and heating processes under 175 °C. The thermodynamic properties of **Rtx12** was characterized by polarized optical microscopy (POM) (**Figure S32**), differential scanning calorimetry (DSC) (**Figure S33**), and variable temperature X-ray diffraction (VT-XRD) (**Figure S34**). The ^1H NMR results of **Rtx12** with different thermal histories (**Figure S35**) provide the thermal stability information.

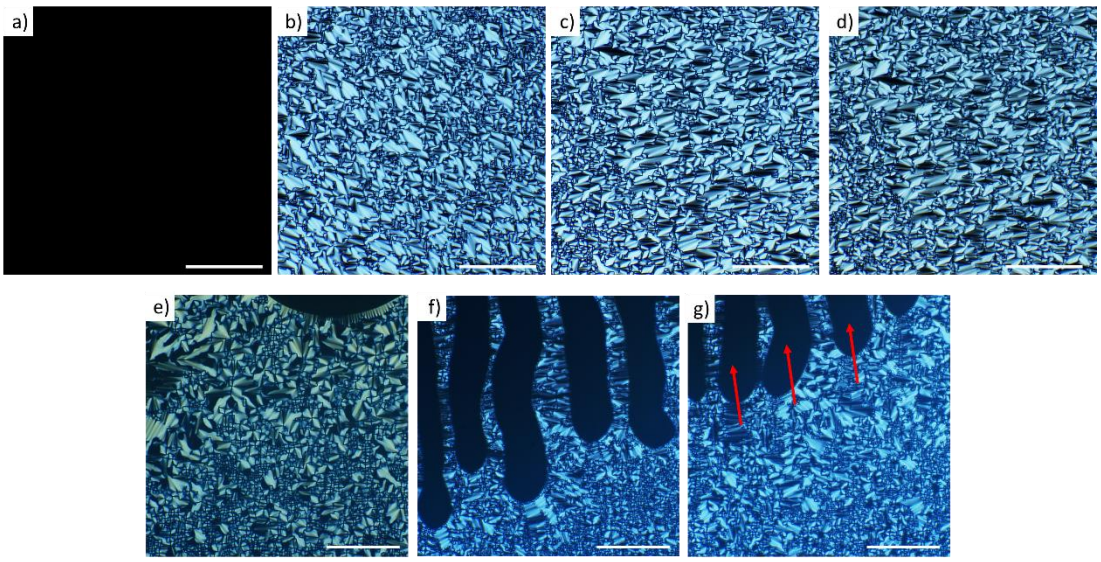

Figure S32. Representative POM images (crossed polarized) of **Rtx12** at a) 165 °C, b) 140 °C, c) 120 °C, and d) 28 °C upon cooling from 170 °C. POM images of **Rtx12** at 140 °C e) before and f) after uniaxial shear application in the vertical direction of the image and g) 10 s after adding shear application. Red arrows in g) indicate the flow direction of **Rtx12**. Scale bars, 100 μm.

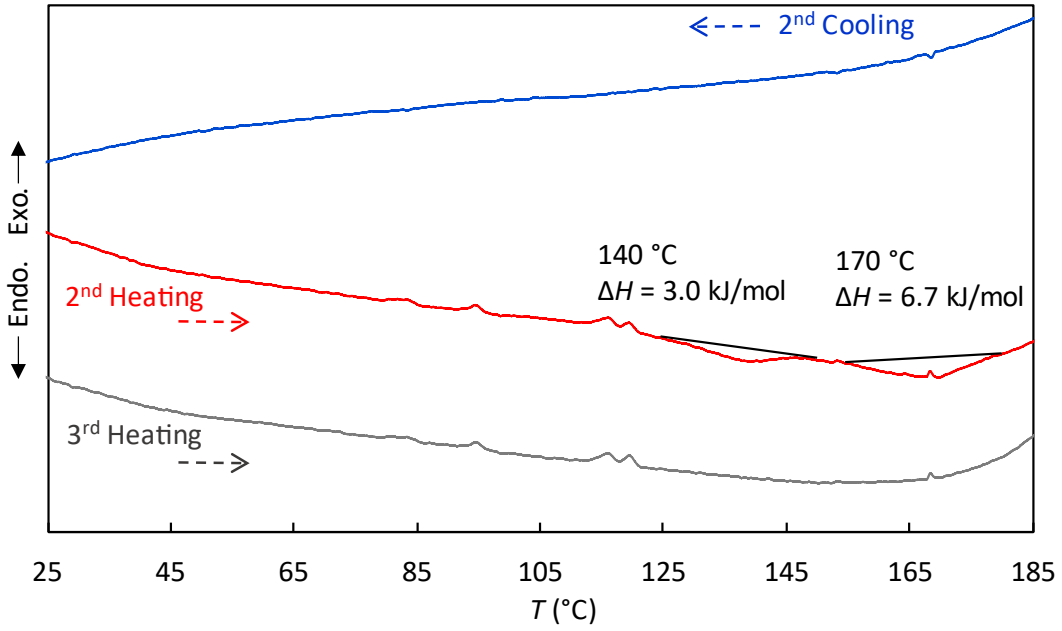

Figure S33. DSC thermograms of **Rtx12** at a scan rate of 10 °C/min under N_2. Two endothermic peaks were observed in the 2nd heating and disappeared in the 3rd heating due to the partial decomposition caused by heating to 190 °C.

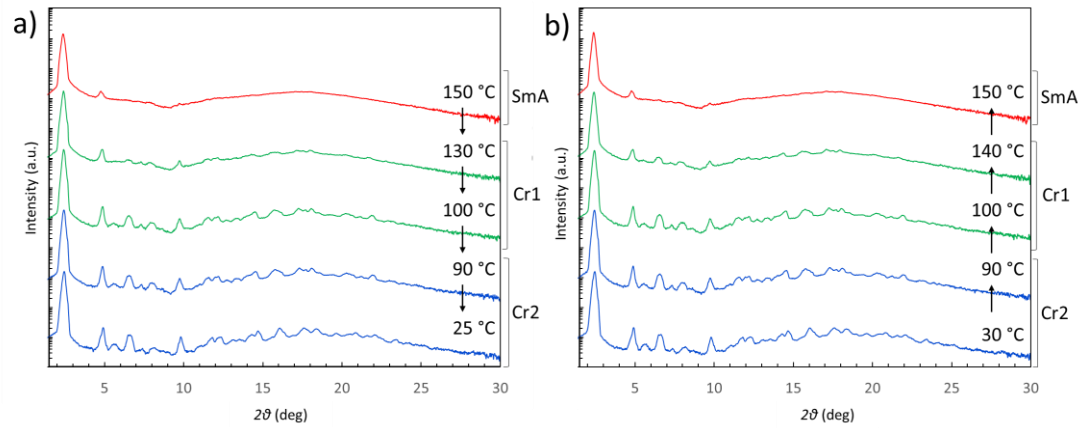

Figure S34. XRD pattern of **Rtx12** a) in the cooling process from 150 °C and b) in the subsequent heating process. The **Rtx12** was placed in a glass capillary filled with argon gas.

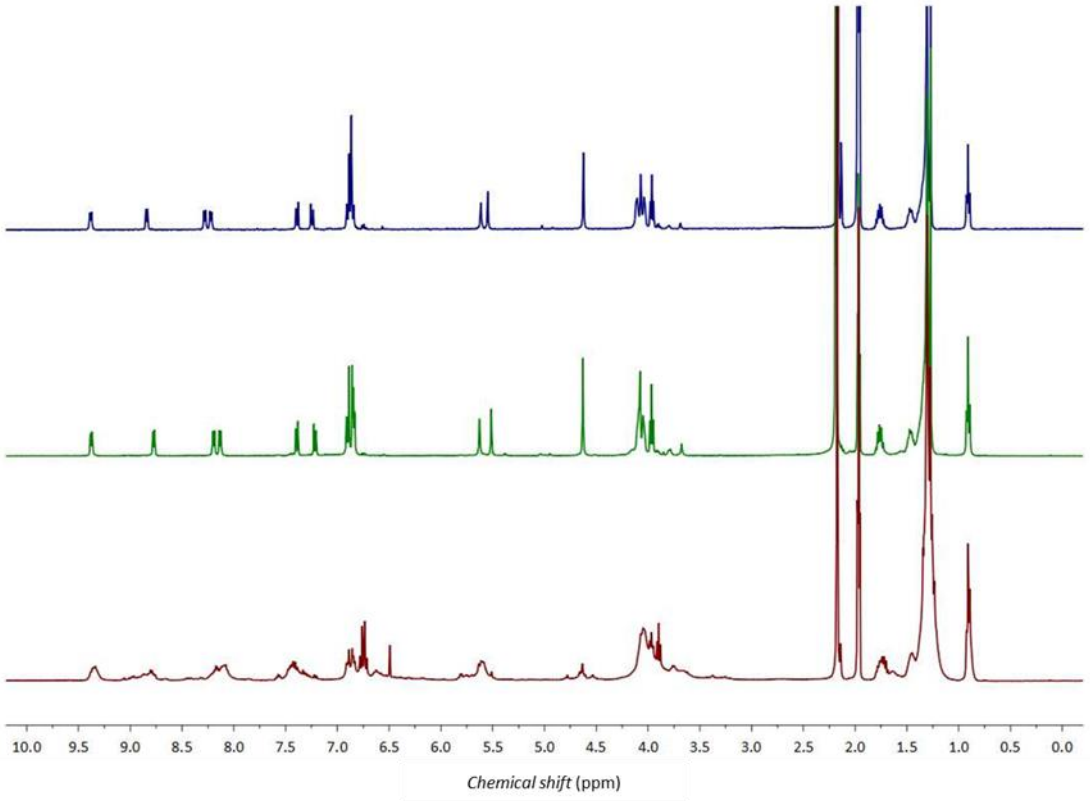

Figure S35. ^{1}H NMR spectrum (400 MHz, 298 K, CD_3CN) of **Rtx12** with different thermal hysteresis: (top) without heating, (middle) after heating at 175 °C, and (bottom) after heating at 190 °C (bottom). Heating was performed by DSC measurement under N_2.

3.2. Structural studies of **Rtx12**

We conducted a DFT calculation to evaluate the stable molecular structure of **Rtx12** (**Figure S36**). To experimentally verify the calculated stable structure, we prepared uniaxially oriented **Rtx12** by shear application and evaluated it by polarized infrared (IR) absorption spectra. As a preliminary step, we characterized the IR spectra of **A1**, **R12**, and **Rtx12** (**Figure S37**). To make a uniaxially oriented **Rtx12** sample,

we placed Rtx12 between two CaF_2 glass slides and then heated it at 150 °C to the SmA phase. At this temperature, we applied uniaxial shear stress to **Rtx12** by repeatedly moving one of the glasses in one direction and then quenched it in air. POM observations of the prepared sample under crossed polarizers displayed a clear contrast at every 45° rotation, and the image became completely dark when the polarization direction and shear indication direction were parallel or perpendicular (**Figure S38a**). This means **Rtx12** was uniaxially oriented in the shear direction. Then, this oriented sample was evaluated by polarized IR to get insight into the anisotropy of the molecular moieties of **Rtx12**. The collected polarized IR spectra (**Figure S38b**) revealed that both the aliphatic alkyl moieties of the ring and the cationic nitrogen-carbon moieties of the axle were aligned parallel to the shear direction. This supports the DFT calculation.
In **Figure S36**, we estimated total molecular length (*L*) was 51.9 Å, which is longer than the layer spacing value (*d*) of 37.1 Å calculated by XRD. This result means **Rtx12** has a double bilayer with an interdigitated structure, represented in **Figure S39**.

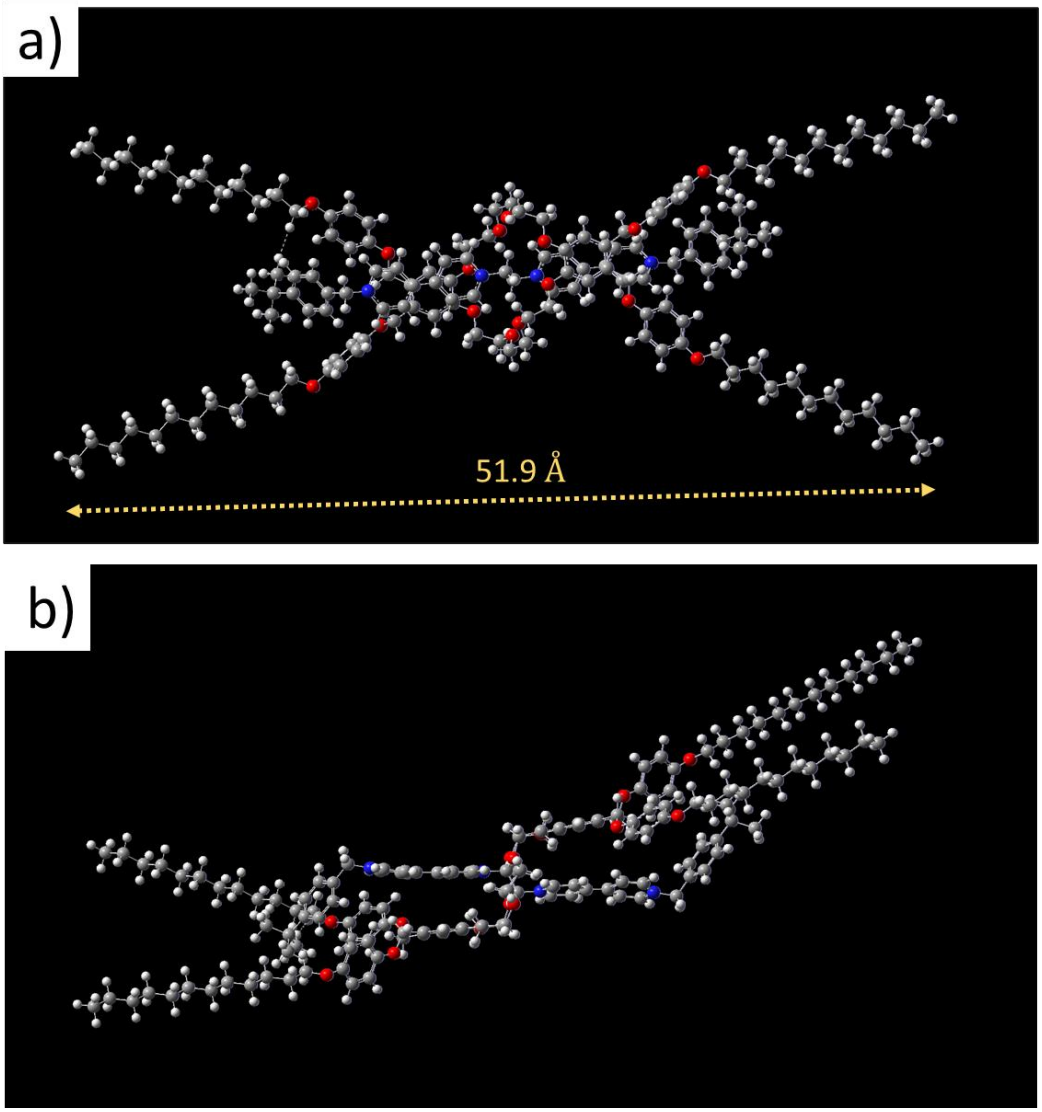

Figure S36. DFT-optimized structure of **Rtx12** using the 6-31g(d, p) basis set with B3LYP; a) top view and b) side view.

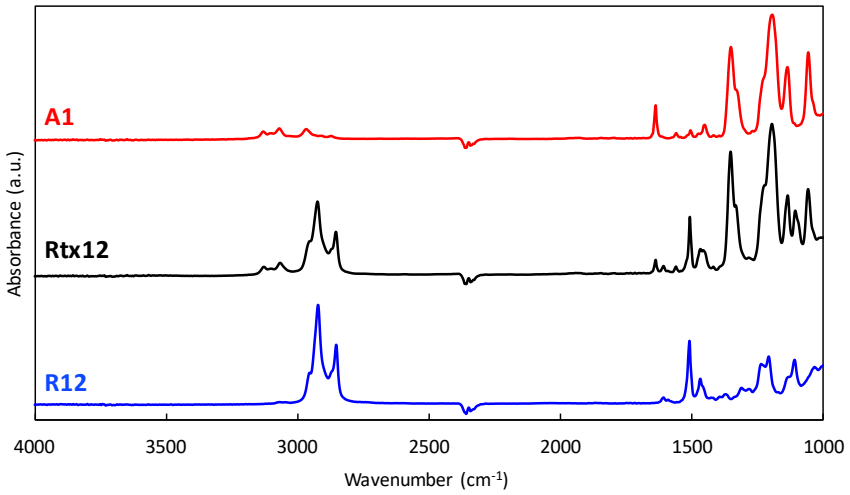

Figure S37. IR spectra of **A1** (top), **Rtx12** (middle), and **R12** (bottom); samples were prepared in films sandwiched between two CaF_2 glass slides. The **Rtx12** spectrum combines characteristics of those of **A1** and **R12**.

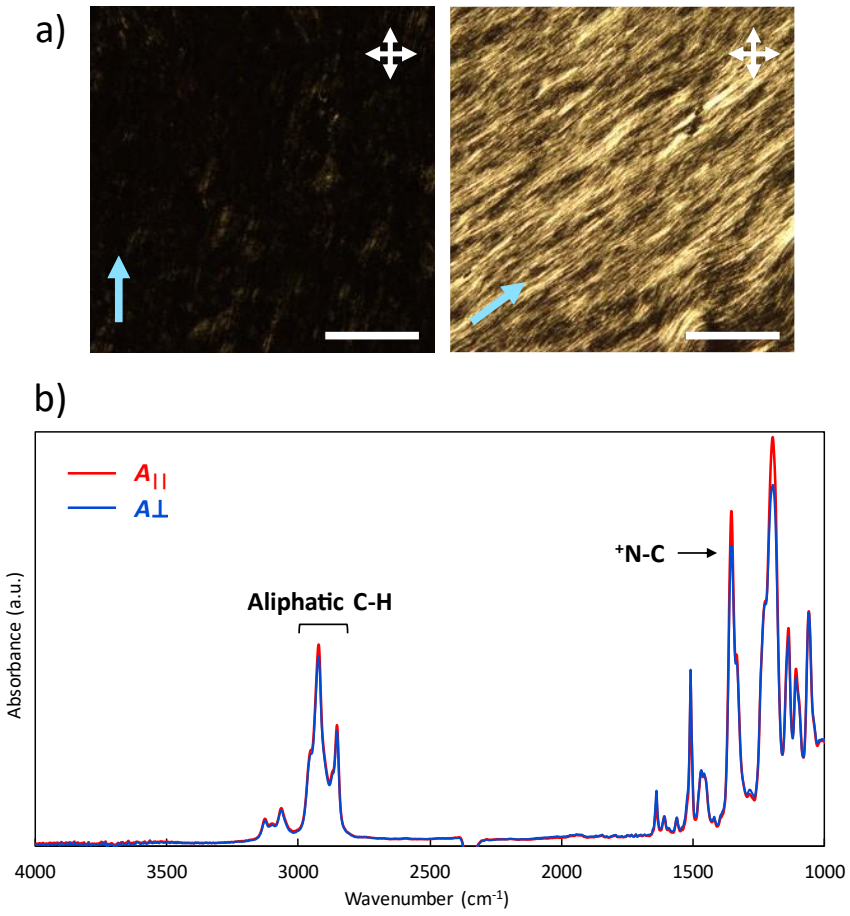

Figure S38. Anisotropy evaluation of uniaxially shear applied **Rtx12**. a) POM images of the **Rtx12** sample rotated by 45° at room temperature. Scale bars, 100 µm. Light blue arrows indicate the shear direction; white arrows depict the direction of the polarizers. b) polarized IR absorption spectra or shear applied **Rtx12**. $A_{||}$ and $A_{\perp}$ are absorption spectra parallel and perpendicular to the shear direction, respectively.

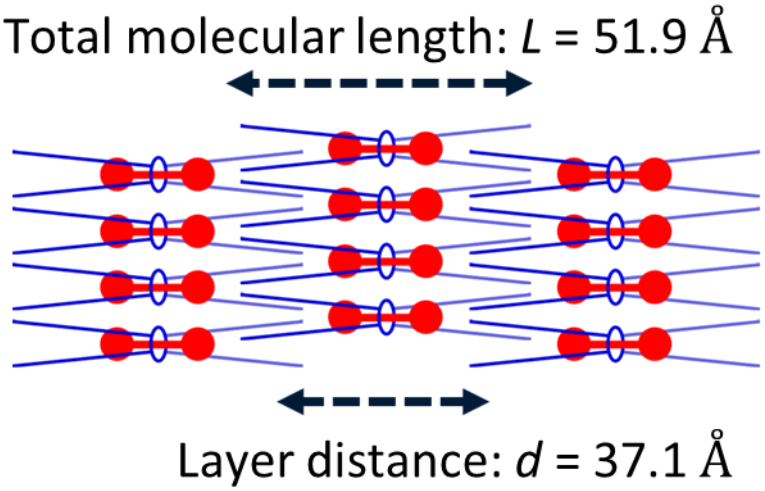

Figure S39. Illustration of possible arrangements of **Rtx12** in the SmA phase.

4. Thermodynamic Studies of Comparisons of Rtx12

To understand the role of [2]rotaxane structure in the emergence of thermotropic LC in **Rtx12**, the thermodynamic properties of the following 3 sets of comparison samples were investigated: i) molecular components (**A1** and **R12**), ii) same chemical components as **Rtx12** without [2]rotaxane structure (equimolar mixture of **A1** and **R12**), and iii) [2]rotaxanes with no or shorter side chains (**Rtx0** and **Rtx6**). The thermodynamic studies were evaluated by DSC, POM, and VT-XRD as needed.

4.1. Thermodynamic properties of **A1**

A1, the axle molecule of **Rtx12**, exhibited no LC phase in DSC, POM, and VT-XRD (**Figure S40** - **Figure S42**) observations upon neither heating nor cooling. In the 1st cooling process of DSC scans from isotropic phase at 200 °C, **A1** was crystallized at 131 °C. In the 2nd heating process **A1** melted at 186 °C to the isotropic phase; however, **A1** showed no signals in the following cooling process. In the POM and VT-XRD results showed the vitrification of **A1** upon cooling from the isotropic phase. For a better understanding, we collected **A1**, which was heated at 200 °C in VT-XRD measurement and analyzed it by ^{1}H NMR. The ^{1}H NMR measurement (**Figure S43**) showed the partial decomposition. Thus, we consider that **A1** heated at 185 °C underwent thermal decomposition and then was vitrified.

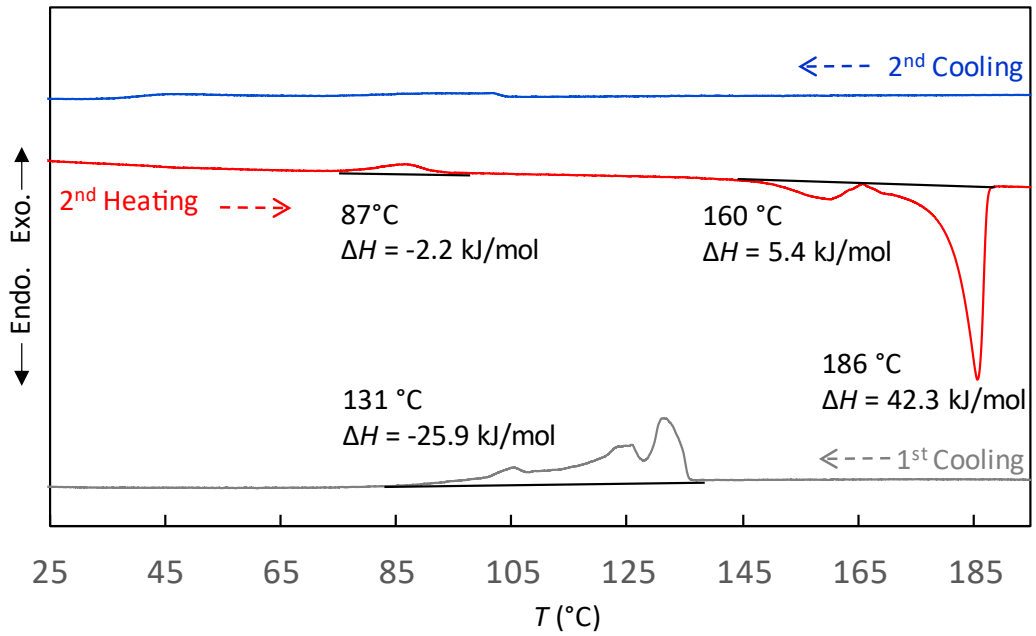

Figure S40. DSC thermograms of **A1** in the 1st cooling, 2nd heating, and 2nd cooling at a scan rate of 10 °C/min under N_2.

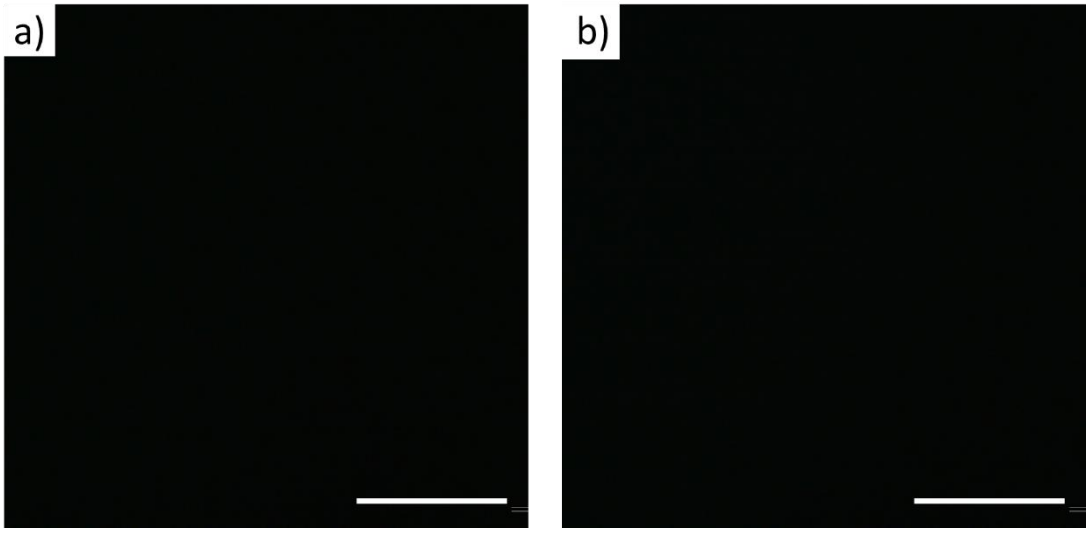

Figure S41. Representative POM images (crossed polarized) of **A1** at a) 200 °C and b) 30 °C upon cooling from 200 °C. Scale bars, 100 µm.

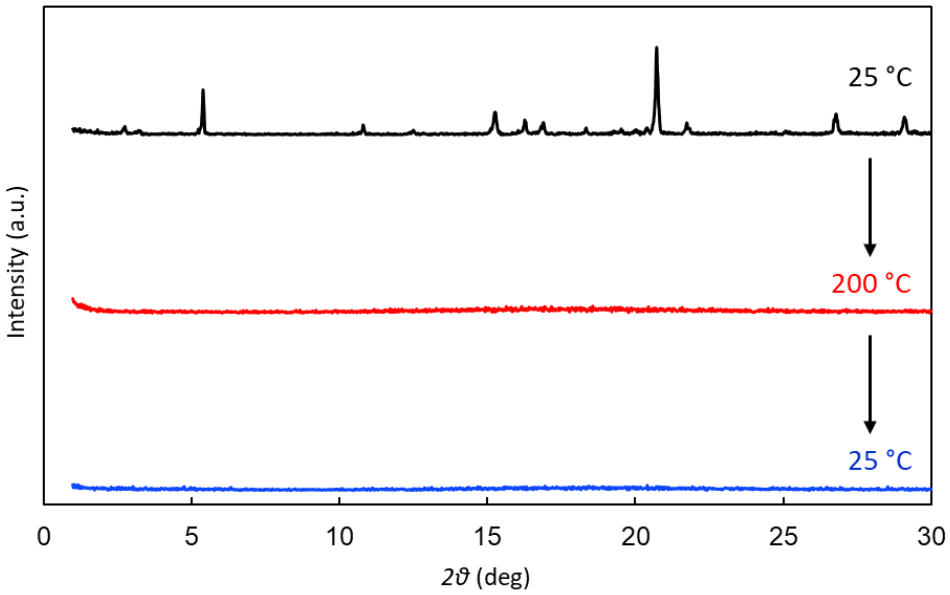

Figure S42. Diffraction patterns of **A1** at (top) 25 °C before heating, (middle) 200 °C, and (bottom) 25 °C after cooling under N_2.

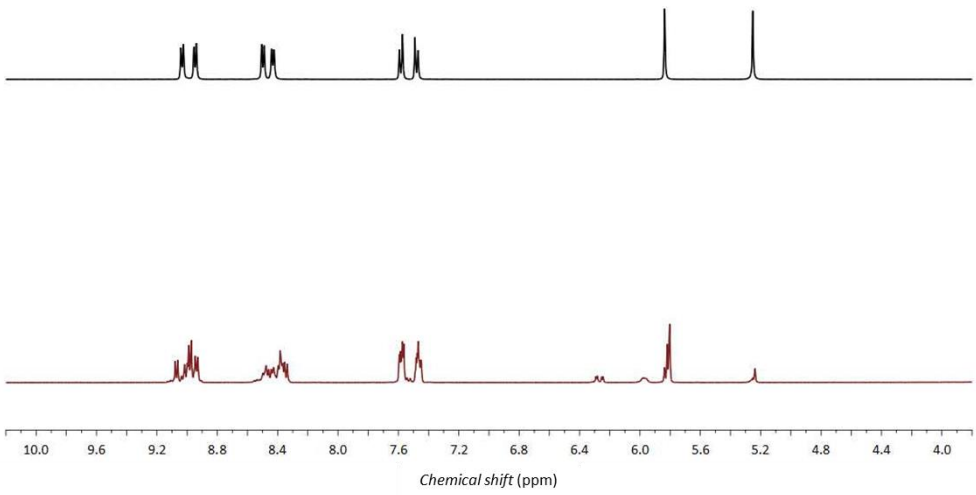

Figure S43. Partial ^{1}H NMR spectrum (400 MHz, 25 °C, CD_3CN) of **A1** before heating (top) and after VT-XRD measurement at 200 °C (bottom).

4.2. Thermodynamic properties of **R12**

The ring molecule **R12**, as a molecular component of **Rtx12**, exhibited a crystalline-isotropic phase transition with no LC phase in DSC thermograms, POM images, and VT-XRD patterns (**Figure S44** - **Figure S46**) upon heating and cooling. Its melting point and crystallization temperature were 67 and 41 °C, respectively.

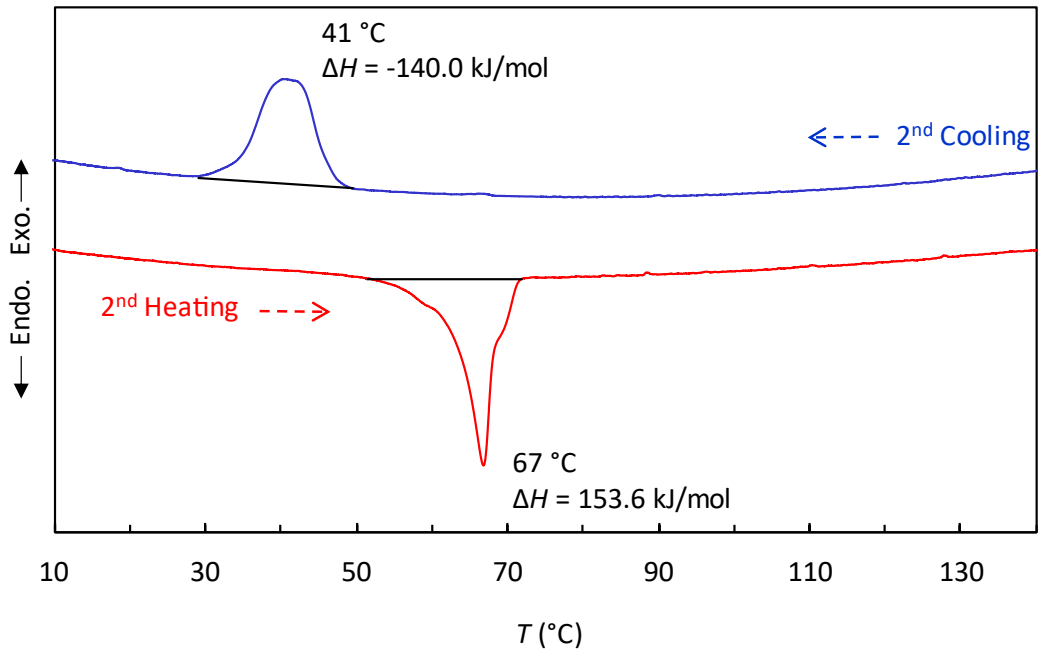

Figure S44. DSC scans of **R12** on 2nd heating and cooling at 10 °C/min under N_2.

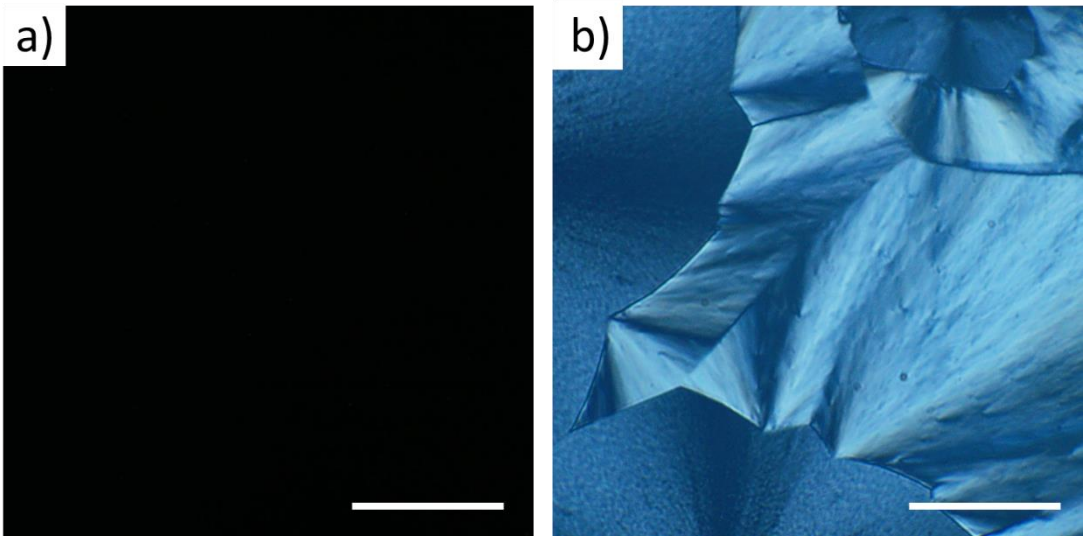

Figure S45. Representative POM images (crossed polarized) of **R12** at a) 90 °C and b) 30 °C upon cooling from 120 °C. Scale bars, 100 µm.

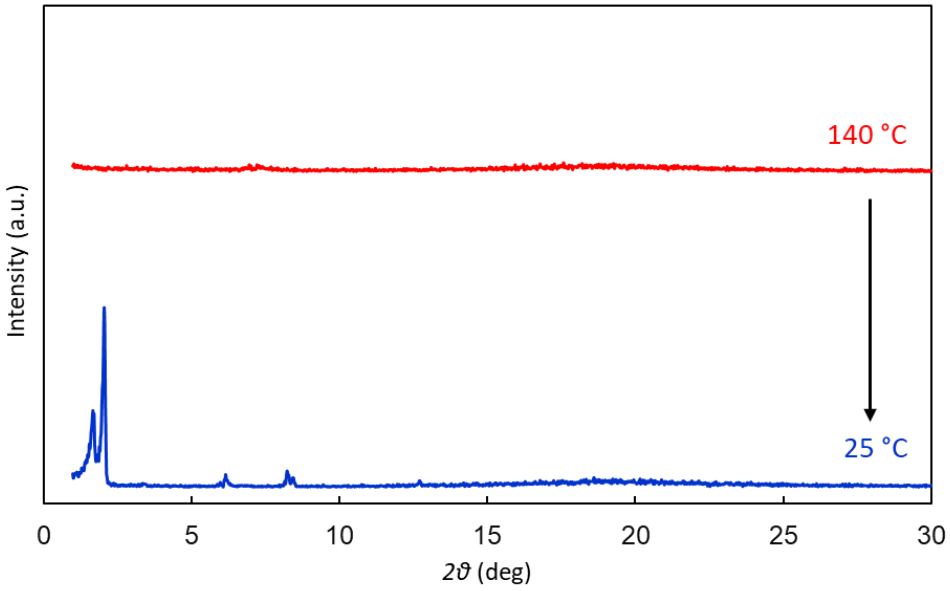

Figure S46. XRD diffraction patterns of **R12** at (top) 140 °C and (bottom) 25 °C upon cooling from 150 °C under N_2.

4.3. Thermodynamic properties of an equimolar mixture of **A1** and **R12**

Equimolar **A1** and **R12** were mixed in $CHCl_3/CH_3CN$ (1:1, v/v, 5 mM), and then all solvents were evaporated under vacuum to afford a solid mixture of **A1** and **R12** in a 1:1 molar ratio. This mixture could not form [2]rotaxane structure, which was evident by ^1H NMR and UV−vis measurements, and exhibited no LC phase. The POM images (**Figure S47**) imply that the crystallization of **R12** and vitrification of **A1** occur independently. The VT-XRD (**Figure S48**) and POM measurements show the absence of the layered structure in **Rtx12** and suggest the crystallization and vitrification upon cooling.

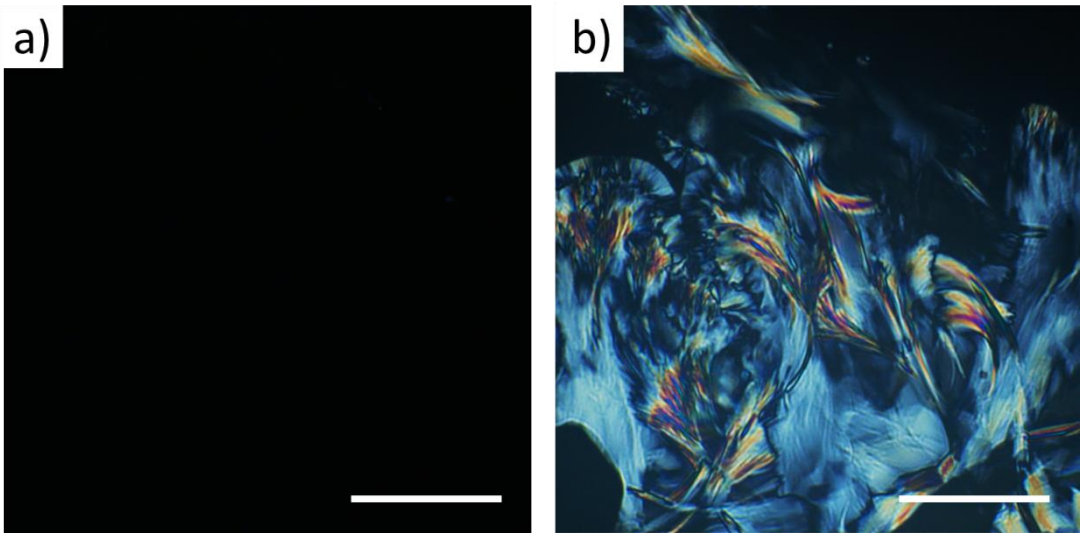

Figure S47. Representative POM images (crossed polarized) of a mixture of **A1** and **R12** (1:1, molar ratio) at (left) 175 °C and (right) 40 °C upon cooling from 200 °C. Scale bars, 100 µm.

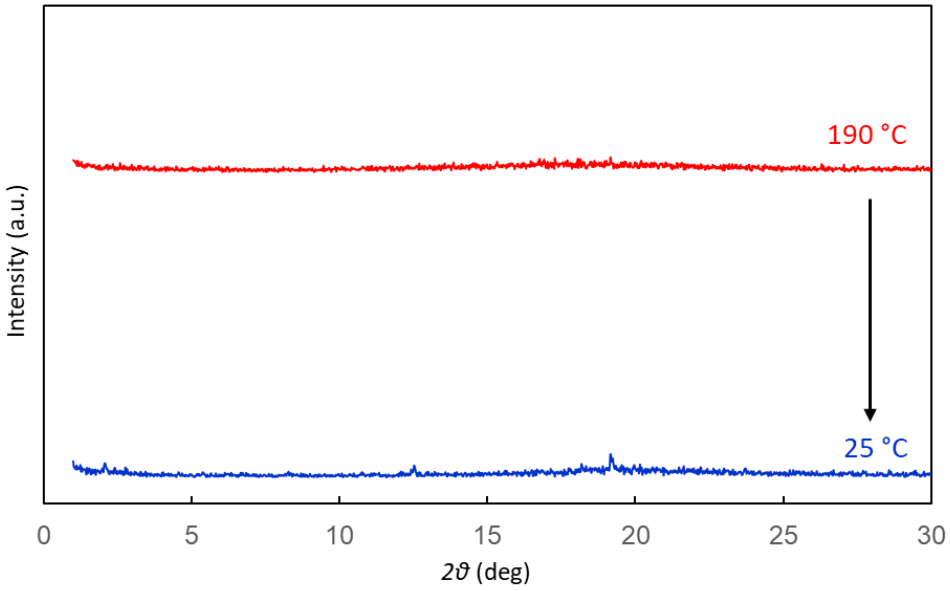

Figure S48. XRD diffraction patterns of an equimolar mixture of **A1** and **R12** at (top) 190 °C and (bottom) 25 °C upon cooling from 190 °C under N_2.

4.4. Thermodynamic properties of **Rtx0**

Rtx0 showed crystalline and isotropic phases but no LC phase from DSC (**Figure S49.** DSC thermograms of Rtx0 **on** 2nd heating and cooling at 10 °C/min under N2and POM (**Figure S50**) measurements.

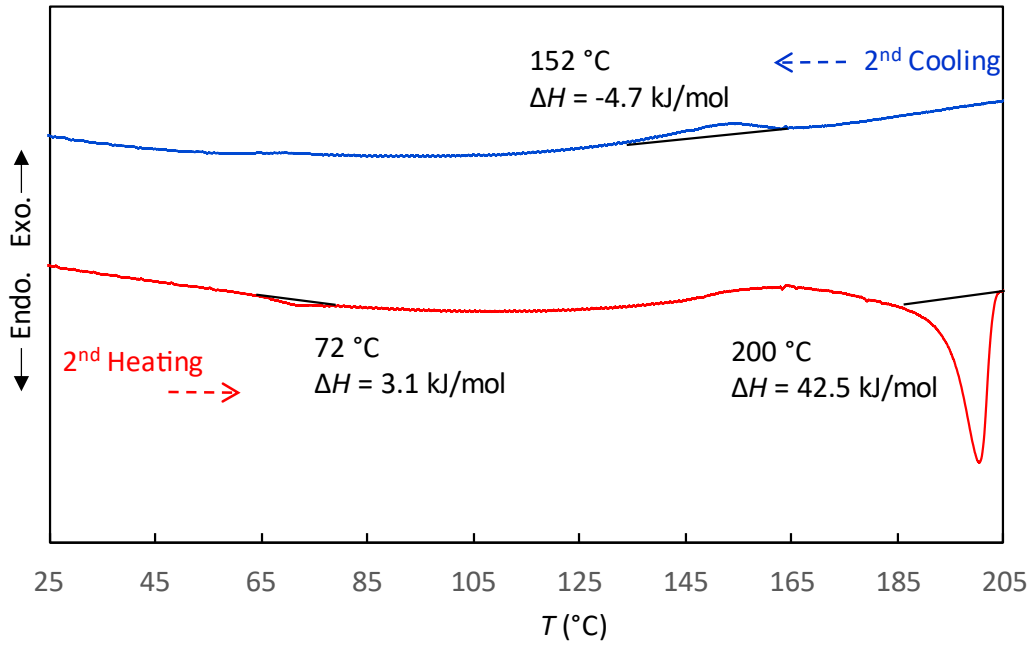

Figure S49. DSC thermograms of **Rtx0** on 2nd heating and cooling at 10 °C/min under N_2.

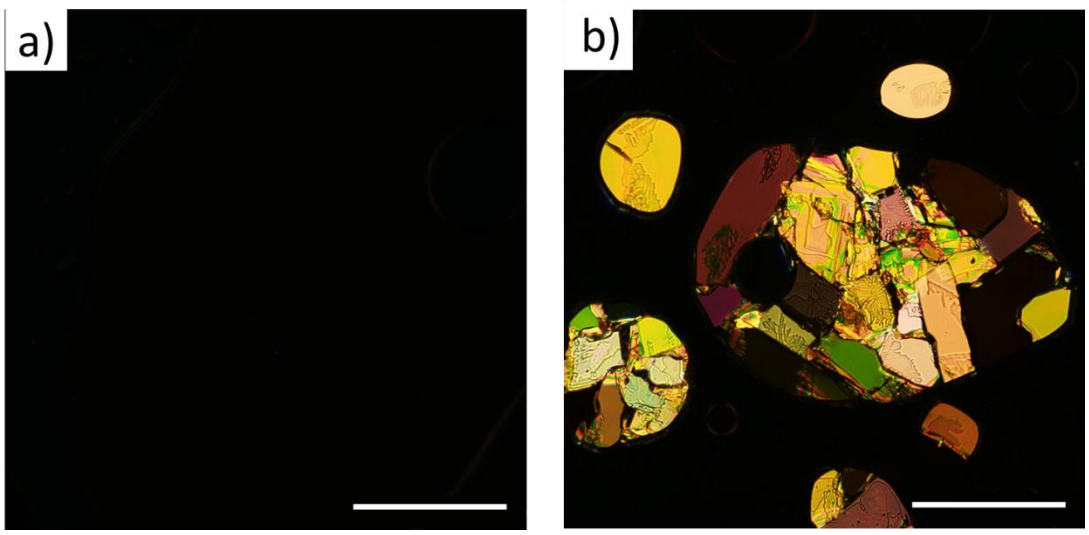

Figure S50. Representative POM images (crossed polarized) of **Rtx0** at (left) 205 °C and (right) 70 °C upon cooling from 210 °C. Scale bars, 200 µm.

4.5. Thermodynamic properties of **Rtx6**

Rtx6 showed crystalline and isotropic phases but no LC phase from DSC (**Figure S51**) and POM (**Figure S52**) measurements.

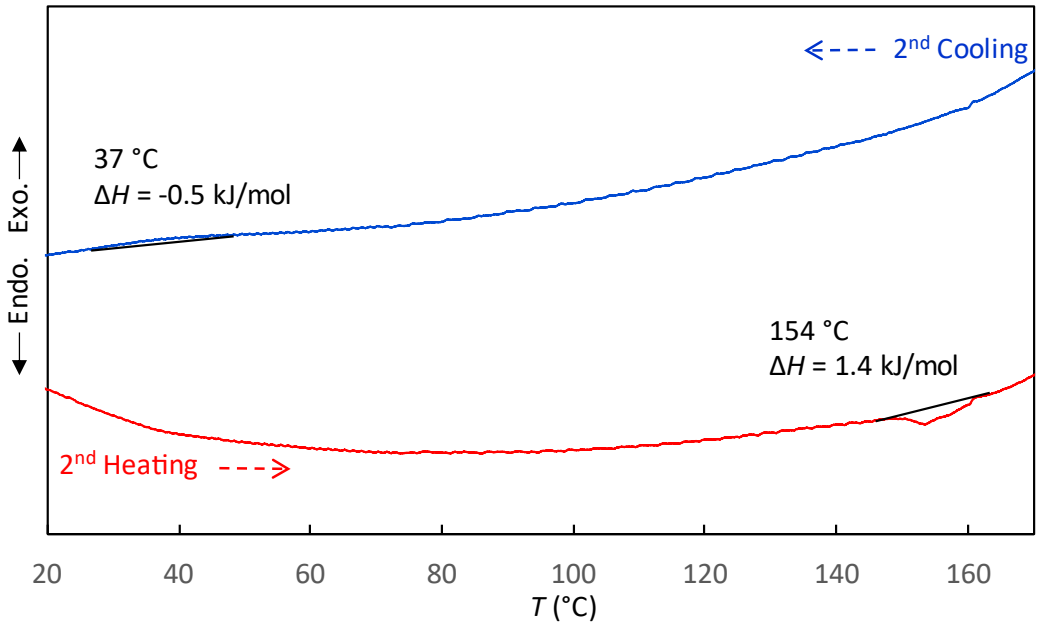

Figure S51. DSC thermograms of **Rtx6** on 2nd heating and cooling at 10 °C/min under N_2.

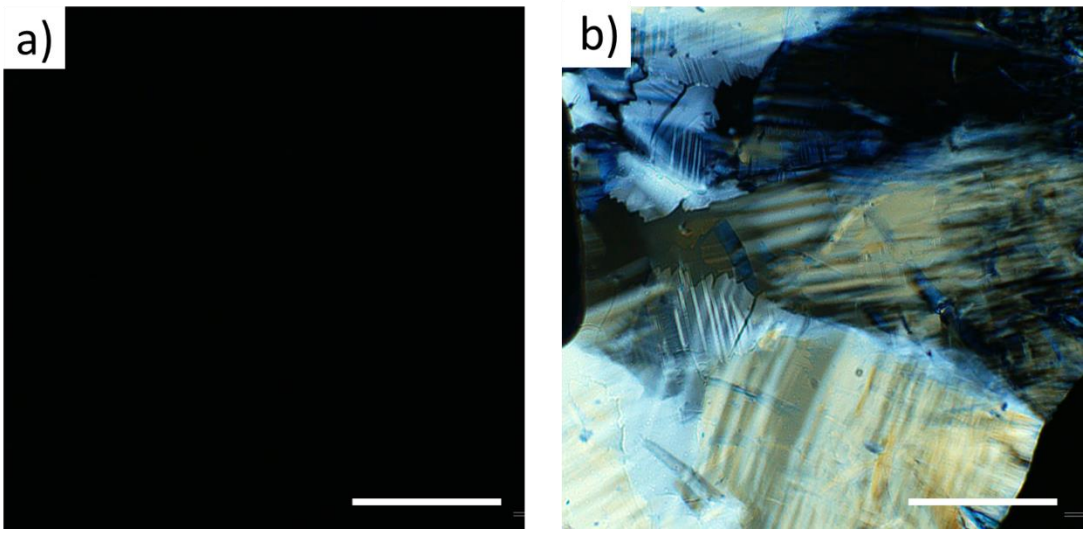

Figure S52. Representative POM images (crossed polarized) of **Rtx6** at a) 160 °C and b) 35 °C upon cooling from 170 °C. Scale bars, 50 µm.

5. References

1 Y. Nakamura, A. Asami, T. Ogawa, S. Inokuma and J. Nishimura, *J. Am. Chem. Soc.*, 2002, **124**, 4329–4335.

2 S. Zhang, K. Luo, H. Geng, H. Ni, H. Wang and Q. Li, *Dalt. Trans.*, 2017, **46**, 899–906.

3 S. J. Loeb, J. Tiburcio, S. J. Vella and J. A. Wisner, *Org. Biomol. Chem.*, 2006, **4**, 667–680.

4 D. J. Mercer, S. J. Vella, L. Guertin, N. D. Suhan, J. Tiburcio, V. N. Vukotic, J. A. Wisner and S. J. Loeb, *Eur. J. Org. Chem.*, 2011, **9**, 1763–1770.